Journal of Sound and Vibration xxx (xxxx) xxx

Contents lists available at ScienceDirect

Journal of Sound and Vibration

journal homepage: www.elsevier.com/locate/jsvi

Optimally tuning an absorber for a chatter-resistant rotating slender milling tool holder

Arjun Patel, Devang kumar Talaviya, Mohit Law *, Pankaj Wahi

Department of Mechanical Engineering, Indian Institute of Technology Kanpur, Kanpur 208016, India

ARTICLE INFO

Keywords:
Chatter
Milling
Absorber
Vibration
Tool holder
Rotor dynamics

ABSTRACT

Machining of parts with deep pockets necessitates the use of long slender milling tooling systems with absorbers integrated within them to make the milling process chatter vibration resistant. As milling tools rotate, their dynamics change with speed. Hence, the use of classical analytical methods of tuning absorbers that presume the primary system to have fixed parameters may result in suboptimal designs. To address this, we present methods to tune an absorber integrated within a rotating milling tool holder while accounting for its speed-dependent characteristics. The milling tool holder is modelled as a rotating cantilevered Euler-Bernoulli beam with small distributed viscous damping and a secondary absorber system attached at a point along its length. The governing equations of motion account for all the artifacts associated with rotation viz. gyroscopic, Coriolis, and the centrifugal effects. Rotational effects couple vibrations in orthogonal planes and make the cross frequency response functions as flexible as the direct ones. Since these speed-dependent dynamic characteristics govern the chatter-free machining stability limits, maximization of this limit is treated as the objective function to find the optimal mass, stiffness, and damping of the absorber. We find that an optimally tuned absorber using the proposed approach results in a~16.5 fold improvement in the chatter-free machining capability as compared to a~11.5 fold improvement using other classical methods of tuning the absorber.

1. Introduction

Milling of parts with deep pockets necessitates the use of long slender milling tooling systems. These slender tools tend to vibrate under the action of cutting forces. These process-induced excitations may result in large amplitude unstable regenerative chatter vibrations that may damage the part quality, the tool, and the machine tool system. Often, the only feasible solutions to mitigate such unwanted vibrations of slender tooling systems are to improve their dynamic stiffness and/or their vibration absorption capacity.

Solutions for milling tooling systems to improve their vibration characteristics have involved the use of holders made of high strength composites [1–3], the use of constrained layer damping in tool holders [4], the use of damped collets inside milling tool holders [5], and the use of damping cores integrated within the tool holders [6,7]. Other solutions have focused on frictional damping within the tool [8,9], and on integrating tuned mass dampers (absorbers) [10–13] with the tool holders. Of these different methods, the methods of integrating absorbers within tooling systems are preferred due to their simple designs and ease of implementation. Further, it has also been established that the tuned absorber is practically viable in industrial settings [14]. Hence, this paper focuses its attention on integrating an optimally tuned absorber within milling tool holders to make them more chatter-resistant.

* Corresponding author.
E-mail address: mlaw@iitk.ac.in (M. Law).

https://doi.org/10.1016/j.jsv.2021.116594
Received 7 July 2021; Received in revised form 18 October 2021; Accepted 28 October 2021
Available online 2 November 2021
0022-460X/

The design of absorbers for tooling systems involves selecting the mass, stiffness, and damping of a secondary oscillator attached to the primary tooling system such that some vibratory energy from the latter is transferred to the former and hence, dissipated from the primary system. While there exist many methods to guide the analytical tuning of absorbers for tooling systems [15–17], all methods of tuning assume the dynamics of the primary system to be constant. While this may hold true for tuning of absorbers for stationary boring tools [18–21], methods of tuning for rotating milling tooling systems in which the dynamics of the primary system change with rotational speed remains largely unexplored.

In recent work, Ma et al. [22] discussed the tuning of an absorber integrated within a milling holder by accounting for the change in the dynamics because of the gyroscopic effects due to rotation. They however ignored potential infleunces of the Coriolis and centrifugal effects. Their work was also limited to tuning the absorber for operation only at a fixed speed. Other recent work discussed the tuning of multiple absorbers to damp a machine tool structural component whose dynamics varied with changing position of the structural component during the cutting process [23]. However, since that work focused on tuning multiple absorbers to damp a structure with varying dynamics during cutting, the method of tuning presented in [23] is not directly relevant to the present case of tuning a single absorber to account for how dynamics changes with speed.

Though examples from other domains exemplify tuning of absorbers while accounting for rotational motion, such as in paper roller machines [24], compressors [25], washing machines [26], as well as in other rotating systems [27], there appears to be no reported work addressing the tuning of absorbers for rotating milling tool holding systems that account for gyroscopic, Coriolis, and centrifugal effects. Since the source of vibrations in milling tool systems is self-excitation primarily due to the regenerative chatter instability arising out of the interactions between the cutting process and the dynamics of the tool which is different from the rotating unbalance in [24–27], the absorber tuning methods reported in [24–27] cannot be directly applied to the problem being studied in the current paper.

The dynamics of rotating milling systems are more complicated than the case when the effects of rotation are ignored [28–34]. The gyroscopic, Coriolis, rotational inertia, and centrifugal effects of the system render the dynamics to be speed-dependent. Due to rotation, each zero-speed vibration mode splits into two for all non-zero speeds. The natural frequency of one mode increases with speed and this is known as the forward wave, and the other backward wave is characterized by natural frequencies that reduce with increasing speeds. Mode splitting also becomes a feature of the dynamics characterized by frequency response functions (FRFs). These FRFs exhibit two peaks for every mode at every non-zero speed as opposed to only a single peak for every mode at zero-speeds. Furthermore, gyroscopic and Coriolis effects couple vibrations in orthogonal planes [29], and this makes the cross FRFs (between directions) as dominant as the direct FRFs [33]. The change of dynamics with speed, combined with the relative magnitudes of both direct and cross FRFs becoming comparable, makes the tuning of an absorber to be integrated somewhere within the tool holder non-trivial. To fill this important technological gap in the existing literature, it is the explicit aim of this paper to present model-based methodologies to help guide the development of chatter-resistant damped milling tool holding systems in which the absorber is tuned accounting for the speed-dependent characteristics of the holder.

The milling holder in this paper is modelled as a cantilevered Euler-Bernoulli beam with small distributed viscous damping as detailed in Section 2. Since the holder is slender, the Euler-Bernoulli beam is thought to be sufficient to capture its deformation behavior [35]. The beam is made locally hollow for a portion along its length to accommodate the absorber within it which is modelled as a lumped mass connected to the beam using a spring and a damper at a single point. This overcomes the shortcomings of other analytical methods that model the primary system as a simple single degree of freedom system and hence presume placement of the absorber at the free end of the beam. Since the free end is also the cutting end, those analytical solutions for tuning of the absorber may result in infeasible design solutions. Our formulation of a continuous beam with a locally hollow section facilitates placement of the absorber anywhere along the length of the holder. The analytical model for the beam presented herein accounts for gyroscopic, Coriolis, rotational inertia, and centrifugal effects. For the absorber, only the Coriolis and centrifugal effects are considered while deriving its governing equations of motion since the gyroscopic and rotational inertia effect drop off due to the assumption of the absorber as a lumped point mass. The governing equations of motion for the beam and the absorber are derived using the extended Hamilton's principle [36].

Section 3 of this paper discusses how the dynamics of the holder without the absorber change with speed. Section 4 motivates the tuning of the absorber while accounting for the speed-dependent dynamic characteristics of the primary system. The maximization of the chatter-free milling stability limit is treated as the objective function to tune the absorber parameters. For characterizing the chatter-free milling stability limits, we use the well-established frequency-domain stability models reported in [37,38]. And, the numerical optimization scheme is based on the minimax method [39]. Section 5 of the paper presents the results of the optimization investigations, and contrasts those results with other methods of tuning that do not account for the speed-dependent dynamics. The main conclusions follow these discussions in Section 6.

2. Analytical model of the rotating milling tool holder integrated with an absorber

This section first discusses the constructional details of a possible design of a milling tool holding system with an absorber integrated within it. This is followed by deriving the governing equations of motion for this system using the extended Hamilton's principle.

2.1. Possible design of a milling tool holding system integrated with an absorber

A possible design of a damped slender milling tool holding system with a tunable absorber integrated within it is shown sche-

matically in Fig. 1(a). The design shown in Fig. 1(a) builds on the successfully prototyped tuned mass damped stationary boring bar reported in [21]. The holder is shown to have a HSK63A type interface, though any other interface is also possible. The holder supports a face mill at its free end. The length from the gage plane is L, and the diameter of the holder is D. The diameter of the face mill may be the same as, or different than, D. The holder body is locally hollow to accommodate the absorber of mass m_d. The absorber is shown supported in two O-rings assumed to be made of linear viscoelastic materials. One O-ring is supported in an adaptor towards the free end of the holder, and the other O-ring is supported in a slider towards the fixed end of the holder. The slider translates inside the cavity using a grub screw type arrangement. The translation of the slider may compress or expand the O-rings, thus changing its stiffness and damping characteristics, and making this a tunable absorber. The absorber mass may also be changed for tuning as necessary. The adaptor is rigidly secured to the tool holder body using screws, and the face mill in turn, is rigidly secured to the adaptor. Torque transmission between the adaptor and the face mill is through the usual driving key type arrangement. The holder body is assumed to be made of steel with density ρ, and an elastic modulus E. Axes nomenclature in Fig. 1 is consistent with convention, in which the tool axis is always taken as Z. Though only a single grub screw is necessary for tuning, to ensure a symmetric design with no imbalances, another grub screw is mounted in a blind threaded hole diametrically opposite to the threaded hole for the tuning arrangement. The blind threaded hole with a grub screw is not shown in Fig. 1(a).

Fig. 1(b) shows an equivalent schematic of the tool holder system to be modelled as a cantilevered Euler-Bernoulli beam with the absorber assumed to be lumped inside the beam at a distance z_d from the fixed end. The actual contact interface between the holder and the machine's spindle is more complex than the clamped boundary condition. The dynamics of the slender cantilevered tool can significantly be influenced by the actual contact conditions, by the tightening torque applied to the holder, and potentially also by the level of cutting force excitations the holder experiences [40]. However, since identifying those contact characteristics requires controlled experimentation [41], and since identification of joint characteristics is a separate research subject by itself, for investigations herein, the tool holder modelled as a clamped-free Euler-Bernoulli beam is thought be adequate. This approximation is consistent with other similar modeling approaches for slender damped tool holding systems [10–11,20–22]. Moreover, if the actual contact characteristics can be identified, incorporating the appropriate boundary conditions in the model is not difficult. And, though the dynamics of the primary system will undoubtedly change, the proposed procedures to tune the absorber will remain the same.

The equivalent beam model assumes the holder can be modelled in three sections. Sections 1 and 3 are solid, and Section 2 is locally

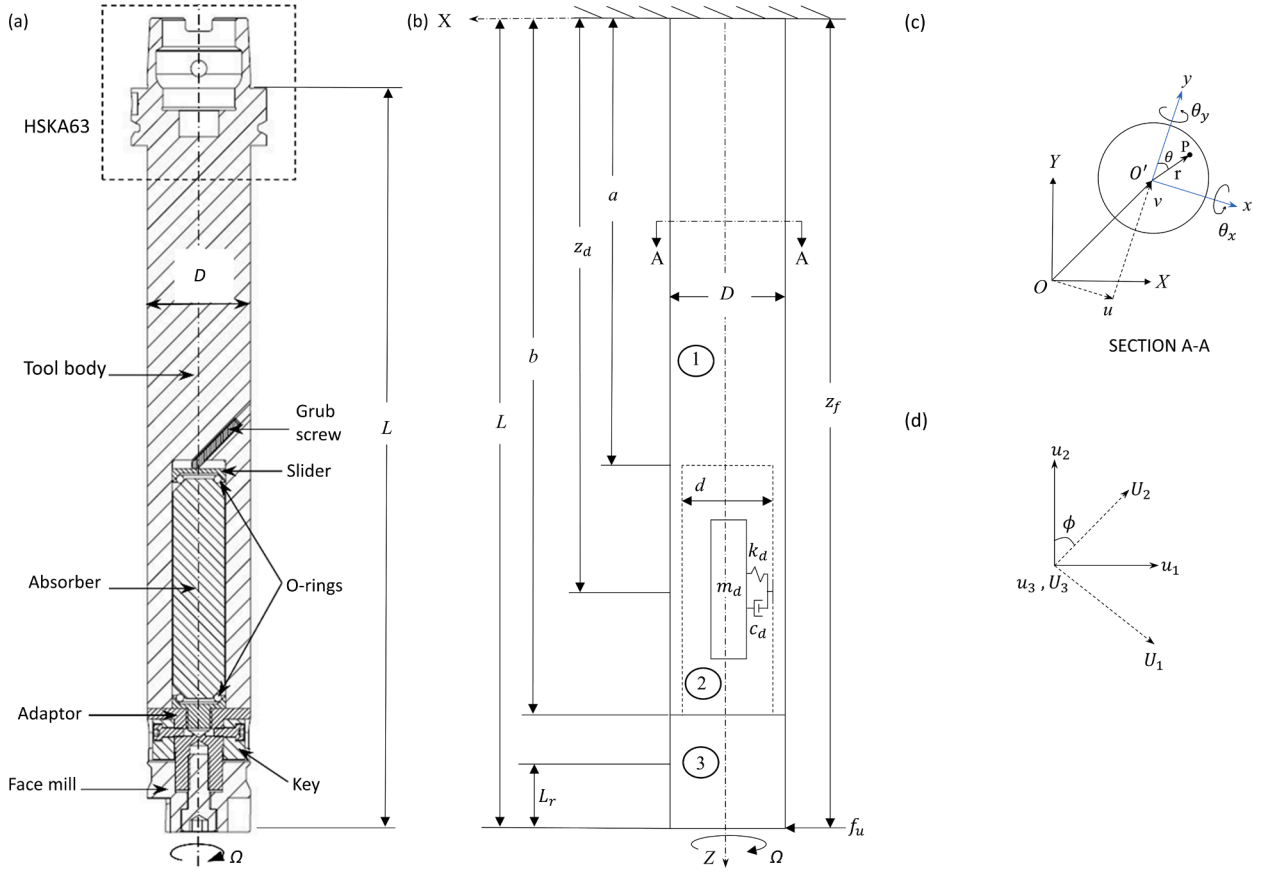

Fig. 1. (a) Possible design of a damped milling tool holding system, (b) Schematic of the equivalent cantilevered beam model with an absorber integrated within, (c) Deflected cross-section of the beam (section A-A) at location z from the fixed end, and (d) Transformation of coordinates from the fixed frame to the rotational frame.

hollow to accommodate the absorber. The hollow cavity starts at a distance a, and ends at a distance b from the fixed end, and has an inner diameter of d. Although the absorber is supported in two O-rings, the model assumes that these two O-rings can be approximated with an equivalent linear stiffness and damping of k_d and c_d, respectively. Since it is difficult to characterize the coupling of the absorber to the beam along its central axis in a 2D representation, Fig. 1(b) instead shows the absorber to be connected to the beam at its inner diameter. The face mill with a diameter of D and length L_r is assumed to be an integral part of tool holder. The milling tool holding system and its equivalent model is assumed to be symmetric about its central axis.

2.2. Derivations of the governing equations of motion

We discuss the energies of the beam and the work done on it, followed by a discussion about the absorber. We then apply the Hamilton's principle to obtain the equation of motion, and then discuss methods of solution for free and forced vibrations.

2.2.1. The beam

The holder and its equivalent uniform beam model are assumed to be spinning about the Z-axis at an angular velocity of Ω rad/s. Since torsional modes are usually dynamically stiffer than the bending ones [35], in the present analysis, only bending flexibilities of the tool holder are considered, and the torsional flexibilities are ignored. Components of the displacement of an arbitrary point P belonging to the beam in the fixed frame $(X-Y-Z)$, are u_1, u_2, and u_3, respectively. At a cross-section z from the fixed end, U_1, U_2, and U_3, are the components of displacement of a general point as measured in the rotating frame $(x-y-z)$, The displacement of the central axis of the beam is assumed to be u and v along the x and y directions of the rotating frame $(x-y-z)$, respectively and θ_x and θ_y are angular deflections in the x and y directions of the rotating frame $(x-y-z)$, respectively. For simplicity, we have assumed that the central axis has no displacement along the $z-$ direction, i.e., $w=0$. Since the cross-section is allowed to rotate or twist about the Z-axis by ϕ ($\dot{\phi}=\Omega$), components of the displaced position vector of a general point P originally at a radius r from the central axis as shown in Fig. 1(c), in the fixed frame of reference can be shown to be:

$$\begin{Bmatrix} x_1 \\ x_2 \\ x_3 \end{Bmatrix} = \begin{bmatrix} \cos\phi & \sin\phi & 0 \\ -\sin\phi & \cos\phi & 0 \\ 0 & 0 & 1 \end{bmatrix} \begin{Bmatrix} r\sin\theta_y\sin\theta_x\cos\theta + r\cos\theta_y\sin\theta + u \\ r\cos\theta_x\cos\theta + v \\ r\cos\theta_y\sin\theta_x\cos\theta - r\sin\theta_y\sin\theta \end{Bmatrix}. \tag{1}$$

From the known position vector, the velocity of the point P can be found, and from that, the kinetic energy of the beam can be defined as:

$$T = \frac{1}{2}\int_0^L \int_0^R \int_0^{2\pi} \rho r\left(\dot{x}_1{}^2 + \dot{x}_2{}^2 + \dot{x}_3{}^2\right) \mathrm{d}r\mathrm{d}\theta\mathrm{d}z. \tag{2}$$

Note that the expression for the kinetic energy above is independent of ϕ as it drops out using trigonometric simplifications. We assume the angular deflections in the x and y directions to be small. As such, $\sin\theta_y \approx \theta_y$, $\sin\theta_x \approx \theta_x, \cos\theta_y \approx 1$ and $\cos\theta_x \approx 1$. The angular deflections of the cross-section of the beam in the $y-z$ plane and in the $x-z$ plane in the rotational frame can be expressed as $\theta_x(z,t) = -\partial v/\partial z$ and $\theta_y(z,t) = \partial u/\partial z$, respectively. By ignoring the cubic and higher orders as well as products of θ_x and θ_y, and by integrating Eq. (2) with respect to θ (from 0 to 2π), and r (from 0 to R, wherein R is the radius of the beam), the kinetic energy of the beam can be shown to be:

$$\begin{aligned} T = \frac{1}{2}\int_0^L \Bigg\{ & \left[\rho A\left(\left(\frac{\partial u}{\partial t}\right)^2 + \left(\frac{\partial v}{\partial t}\right)^2 + 2\Omega\left(v\frac{\partial u}{\partial t} - u\frac{\partial v}{\partial t}\right) + \Omega^2\left(u^2+v^2\right)\right) + \rho I_p\Omega^2\right] \\ & + \rho I\left[\left(\frac{\partial^2 u}{\partial t\partial z}\right)^2 + \left(\frac{\partial^2 v}{\partial t\partial z}\right)^2\right] + 2\rho I_p\Omega\left[\left(\frac{\partial v}{\partial z}\frac{\partial^2 u}{\partial t\partial z} - \frac{\partial u}{\partial z}\frac{\partial^2 v}{\partial t\partial z}\right)\right]\Bigg\}\mathrm{d}z, \end{aligned} \tag{3}$$

wherein A is the area of cross-section of the beam, I is the diametrical area moment of inertia, and I_p is the polar moment of inertia. Note that A, I and I_p are all possible functions of z to account for the variation of the cross-sectional properties of the beam along its length. The kinetic energy expression above incorporates the influence of the Coriolis, centrifugal, rotational kinetic energy, rotational inertia, and gyroscopic terms. Only centrifugal effects resulting from the deflection of the central axis of the rotating beam about the axis of rotation were considered. Influence of runout on the centrifugal forces are presently ignored.

For obtaining the potential energy, we assume that the beam cross-section remains plane after deformation and all the other kinematic relations assumed for the Euler-Bernoulli beam are valid [35,36]. As such, the displacements of a generic point P (from [35, 36]) in the rotational frame $(x-y-z)$ can be written as:

$$\begin{aligned} U_1(x,y,z,t) &= r\sin\theta_y\sin\theta_x\cos\theta + r\cos\theta_y\sin\theta + u(z,t) - r\sin\theta; \\ U_2(x,y,z,t) &= r\cos\theta_x\cos\theta + v(z,t) - r\cos\theta; \\ U_3(x,y,z,t) &= r\cos\theta_y\sin\theta_x\cos\theta - r\sin\theta_y\sin\theta. \end{aligned} \tag{4}$$

Using the notions of linear strains and stresses, and since the beam is assumed symmetric about its central axis, strains of point P can be

expressed as:

$$\varepsilon_{xx} = \frac{\partial U_1}{\partial x};$$

$$\varepsilon_{yy} = \frac{\partial U_2}{\partial y};$$

$$\varepsilon_{zz} = \frac{\partial U_3}{\partial z};$$

$$\varepsilon_{xy} = \frac{\partial U_2}{\partial x} + \frac{\partial U_1}{\partial y};$$

$$\varepsilon_{yz} = \frac{\partial U_3}{\partial y} + \frac{\partial U_2}{\partial z};$$

$$\varepsilon_{zx} = \frac{\partial U_1}{\partial z} + \frac{\partial U_3}{\partial x}. \tag{5}$$

In Eq. (5), strains are written in Cartesian coordinates while displacements of P are in polar coordinates therefore a proper conversion has been made as $r\sin\theta = x$ and $r\cos\theta = y$ in Eq. (4) before taking the derivatives. Under the assumptions of small angular deflections in the x and y directions, we have $\sin\theta_y \approx \theta_y$, $\sin\theta_x \approx \theta_x, \cos\theta_y \approx 1$ and $\cos\theta_x \approx 1$. This makes the shear strain $\varepsilon_{xy} = 0$, while the shear strains ε_{yz} and ε_{zx} are quadratic in θ_y and θ_x, and, as such can be dropped in a linear formulation as ours. Accordingly, the only non-zero strain to be considered for our problem is ε_{zz} for which the potential energy U of the beam can be written as [36]:

$$U = \frac{1}{2}\int_0^L \int_A E\, \varepsilon_{zz}^2 \mathrm{d}A\mathrm{d}z, \tag{6}$$

wherein E is the modulus of elasticity. Substituting Eqs. (4) and (5) in (6) and integrating over the cross-sectional area, we get:

$$U = \frac{1}{2}\int_0^L \left[EI\left(\frac{\partial^2 u}{\partial z^2}\right)^2 + EI\left(\frac{\partial^2 v}{\partial z^2}\right)^2 \right] \mathrm{d}z, \tag{7}$$

wherein EI is the bending rigidity in both planes.

Assuming there to be internal damping within the beam, the work done on the beam by those damping forces can be written as:

$$W_{f1} = \int_0^L (f_{u1}u + f_{v1}v)\mathrm{d}z, \tag{8}$$

wherein f_{u1} and f_{v1} are the damping forces on the beam in the x and the y directions in the rotational frame, respectively. Also, the work done by the damping forces of the absorber on the beam can be written as:

$$W_{f2} = \int_0^L (f_{u2}u + f_{v2}v)\delta(z - z_d)\mathrm{d}z, \tag{9}$$

wherein f_{u2} and f_{v2} are the damping forces on the absorber in the x and in the y directions in the rotational frame, respectively, and δ is the Dirac delta function, used because of our assumption of the absorber being lumped at a single location at a distance z_d from the clamped end.

Furthermore, since forces generated during the cutting process act on the tool, the work done on the beam by these external forces can be written as:

$$W_{f3} = \int_0^L (f_{u3}u + f_{v3}v)\delta(z - z_f)\mathrm{d}z, \tag{10}$$

wherein f_{u3} and f_{v3} are the external forces acting on the beam in the x and the y directions in the rotational frame, respectively and the Dirac delta function accounts for the fact that the cutting forces are acting at a single point located at a distance z_f from the clamped end.

2.2.2. The absorber

Since the absorber is assumed attached along the central axis of the beam, it rotates with the same angular velocity as that of the beam. The absorber's deflections may hence similarly be defined as u_{d1} and u_{d2} in the fixed frame, and as u_d and v_d in the rotational frame, respectively. The transformations between these frames will remain similar to the ones shown in Fig. 1(d). And, since the absorber is modelled as a lumped mass fixed to be beam at z_d, its kinetic energy T_d can be shown to be:

$$T_d = \frac{1}{2}\int_0^L \left\{ m_d \left[\left(\frac{\partial u_d}{\partial t}\right)^2 + \left(\frac{\partial v_d}{\partial t}\right)^2 + 2\Omega\left(u_d\frac{\partial v_d}{\partial t} - v_d\frac{\partial u_d}{\partial t}\right) + \Omega^2\left(u_d{}^2 + v_d{}^2\right) \right] + J_d\Omega^2 \right\} \delta(z-z_d)\mathrm{d}z, \tag{11}$$

wherein J_d is the polar moment of inertia of the absorber.

The potential energy of the absorber can be written as:

$$U_d = \frac{1}{2}\int_0^L k_d\left[(u_d-u)^2 + (v_d-v)^2\right]\delta(z-z_d)\mathrm{d}z, \tag{12}$$

and, the work done on the absorber by the damping forces of the absorber can be written as:

$$W_{f4} = \int_0^L (f_{u4}u_d + f_{v4}v_d)\delta(z-z_d)\mathrm{d}z. \tag{13}$$

wherein f_{u4} and f_{v4} are the damping forces of the absorber in the x and the y directions in the rotational frame, respectively.

2.2.3. The extended Hamilton's principle

Having defined the energies of the beam and of the absorber, and having defined the work done on the system, application of the generalized extended Hamilton's principle states that:

$$\delta_v \int_{t_1}^{t_2} \left(T + W_{f1} + W_{f2} + W_{f3} + W_{f4} + T_d - U - U_d\right)\mathrm{d}t = 0, \tag{14}$$

wherein t_1 and t_2 are the time intervals in the dynamic trajectory, and δ_v is the variational operator. Substituting Eq. (4 – 14) and using the variational operator, and integrating each term by parts, the governing differential equations of motion of the rotating beam and of the absorber can be shown to be:

$$\begin{aligned}
&\rho A\left(\frac{\partial^2 u}{\partial t^2}\right) + 2\rho A\Omega\left(\frac{\partial v}{\partial t}\right) - \rho A\Omega^2 u - \rho I\left(\frac{\partial^4 u}{\partial t^2\partial z^2}\right) - 2\rho I_p\Omega\left(\frac{\partial^3 v}{\partial t\partial z^2}\right) + EI\left(\frac{\partial^4 u}{\partial z^4}\right) + k_d(u-u_d)\delta(z-z_d) \\
&\quad = f_{u1} + f_{u2}\delta(z-z_d) + f_{u3}\delta\left(z-z_f\right); \\
&\rho A\left(\frac{\partial^2 v}{\partial t^2}\right) - 2\rho A\Omega\left(\frac{\partial u}{\partial t}\right) - \rho A\Omega^2 v - \rho I\left(\frac{\partial^4 v}{\partial t^2\partial z^2}\right) + 2\rho I_p\Omega\left(\frac{\partial^3 u}{\partial t\partial z^2}\right) + EI\left(\frac{\partial^4 v}{\partial z^4}\right) + k_d(v-v_d)\delta(z-z_d) = f_{v1} + f_{v2}\delta(z-z_d) + f_{v3}\delta\left(z-z_f\right); \\
&m_d\left(\frac{\partial^2 u_d}{\partial t^2}\right) + 2m_d\Omega\left(\frac{\partial v_d}{\partial t}\right) - m_d\Omega^2 u_d + k_d(u_d-u)\delta(z-z_d) = f_{u4}; \\
&m_d\left(\frac{\partial^2 v_d}{\partial t^2}\right) - 2m_d\Omega\left(\frac{\partial u_d}{\partial t}\right) - m_d\Omega^2 v_d + k_d(v_d-v)\delta(z-z_d) = f_{v4}.
\end{aligned} \tag{15}$$

wherein the first two equations represent the equations of motion of the beam in the x and the y directions, respectively, and the other two represent the equations of motion of the absorber, also in the x and the y directions, respectively. Note that the first two equations are partial differential equations and require appropriate boundary conditions for complete description of the problem. We have assumed an idealized cantilevered boundary condition, i.e., the beam is fixed at one end while it is free at the other end, for simplicity. The second, third, fourth, and fifth terms of the first two equations represent the Coriolis, centrifugal, rotational inertia, and gyroscopic effects of the beam. And, similarly, the second and the third terms in the absorber's equations represent the Coriolis and centrifugal effects of the absorber.

Assuming that the beam's damping can be represented with a coefficient C, and that the absorber's is c_d, Eq. (15) can be updated to account for the influence of damping by assuming the damping forces to take the form of $f_{u1} = -\frac{C}{L}\left(\frac{\partial u}{\partial t}\right)$; $f_{v1} = -\frac{C}{L}\left(\frac{\partial v}{\partial t}\right)$; $f_{u2} = -f_{u4} = -c_d\left(\frac{\partial u}{\partial t} - \frac{\partial u_d}{\partial t}\right)$; $f_{v2} = -f_{v4} = -c_d\left(\frac{\partial v}{\partial t} - \frac{\partial v_d}{\partial t}\right)$. Substituting these forces in Eq. (15), makes the equations of motion:

$$\begin{aligned}
&\rho A\left(\frac{\partial^2 u}{\partial t^2}\right) + \frac{C}{L}\left(\frac{\partial u}{\partial t}\right) + 2\rho A\Omega\left(\frac{\partial v}{\partial t}\right) - \rho A\Omega^2 u - \rho I\left(\frac{\partial^4 u}{\partial t^2\partial z^2}\right) - 2\rho I_p\Omega\left(\frac{\partial^3 v}{\partial t\partial z^2}\right) \\
&+EI\left(\frac{\partial^4 u}{\partial z^4}\right) + \left[k_d(u-u_d) + c_d\left(\frac{\partial u}{\partial t} - \frac{\partial u_d}{\partial t}\right)\right]\delta(z-z_d) = f_{u3}\left(z_f, t\right);
\end{aligned}$$

$$\rho A\left(\frac{\partial^2 v}{\partial t^2}\right)+\frac{C}{L}\left(\frac{\partial v}{\partial t}\right)-2\rho A\Omega\left(\frac{\partial u}{\partial t}\right)-\rho A\Omega^2 v-\rho I\left(\frac{\partial^4 v}{\partial t^2\partial z^2}\right)+2\rho I_p\Omega\left(\frac{\partial^3 u}{\partial t\partial z^2}\right)$$

$$+EI\left(\frac{\partial^4 v}{\partial z^4}\right)+\left[k_d(v-v_d)+c_d\left(\frac{\partial v}{\partial t}-\frac{\partial v_d}{\partial t}\right)\right]\delta(z-z_d)=f_{v3}(z_f,t);$$

$$m_d\left(\frac{\partial^2 u_d}{\partial t^2}\right)+2m_d\Omega\left(\frac{\partial v_d}{\partial t}\right)-m_d\Omega^2 u_d+\left[k_d(u_d-u)+c_d\left(\frac{\partial u_d}{\partial t}-\frac{\partial u}{\partial t}\right)\right]\delta(z-z_d)=0;$$

$$m_d\left(\frac{\partial^2 v_d}{\partial t^2}\right)-2m_d\Omega\left(\frac{\partial u_d}{\partial t}\right)-m_d\Omega^2 v_d+\left[k_d(v_d-v)+c_d\left(\frac{\partial v_d}{\partial t}-\frac{\partial v}{\partial t}\right)\right]\delta(z-z_d)=0. \tag{16}$$

2.2.4. Modal analysis to obtain the reduced equations of motion

We first obtain the mode-shapes associated with the various natural vibration modes of the continuous beam so that we can project the equations of motion for the transverse displacement of the beam's central axis to the modal space. These mode shapes are defined for the zero rotational speed case with no damping and are assumed to be valid for every non-zero speed too. Since the beam is symmetric about its central axis, assuming solutions for the beam deflection in both directions as:

$$u=\sum_j q_{uj}(t)\psi_{sj}(z), \tag{17}$$

wherein $u\equiv v$, and wherein ψ_{sj} are the mode shapes of the beam, and the value of 's' depends on the part/section of the beam considered, i.e., 1, 2, or 3 (see Fig. 1(b) for section numbering). $q_{uj}(t)$ within Eq. (17) represents the time component of the displacements, and 'j' within Eq. (17) represents the mode number.

For each mode shape, the functional description of the displacements for all three parts of the beam are different, and can be represented as [36]:

$$\psi_s=C_{1s}\cos(\beta_s z)+C_{2s}\cosh(\beta_s z)+C_{3s}\sin(\beta_s z)+C_{4s}\sinh(\beta_s z)$$

$$s=\begin{cases}1, & 0\le z\le a\\ 2, & a<z\le b\\ 3, & b<z\le L.\end{cases} \tag{18}$$

The natural frequency of the beam for each mode is defined as [36]:

$$\omega=\beta_1^2\sqrt{\frac{EI_1}{\rho A_1}}=\beta_2^2\sqrt{\frac{EI_2}{\rho A_2}}=\beta_3^2\sqrt{\frac{EI_3}{\rho A_3}}, \tag{19}$$

and because of $I_1=I_3$ and $A_1=A_3$, the relationships between β_1, β_2 and β_3 for each mode are:

$$\beta_2=\beta_1\left[\frac{I_1A_2}{I_2A_1}\right]^{\frac{1}{4}},\beta_1=\beta_3. \tag{20}$$

Solutions for the unknown coefficients C_{is}, $i=1,2,3,4$ and $s=1,2,3$ can be obtained by applying the appropriate boundary conditions at the fixed and free ends and the continuity conditions at the two interfaces between the different sections. At the fixed end, the slope and deflection are zero, i.e.,

$$\psi_1(0)=0;\ \psi_1'(0)=0, \tag{21}$$

and, the bending moment and shear forces are zero at the free end, i.e.,

$$EI_3\psi_3''(L)=0;\ EI_3\psi_3'''(L)=0, \tag{22}$$

wherein'', '$\prime\prime$', and '$\prime\prime\prime$' denote the derivatives with respect to 'z'.

Since the beam has three sections, compatibility conditions at the interfaces of $z=a$ and $z=b$ distances from the fixed end for ensuring continuity of displacements, slopes, shear forces and bending moments around the interfaces are:

$$\psi_1(a^-)=\psi_2(a^+);\ \psi_2(b^-)=\psi_3(b^+);$$

$$\psi_1'(a^-)=\psi_2'(a^+);\ \psi_2'(b^-)=\psi_3'(b^+);$$

$$EI_1\psi_1''(a^-)=EI_2\psi_2''(a^+);EI_2\psi_2''(b^-)=EI_3\psi_3''(b^+);$$

$$EI_1\psi_1''(a^-) = EI_2\psi_2''(a^+);\ EI_2\psi_2''(b^-) = EI_3\psi_3''(b^+); \tag{23}$$

wherein the superscripts '-' and '+' denote the positions slightly before and slightly after the interfacial point(s).

The relationship between the twelve unknowns in the mode shape expression in Eq. (18) are obtained by using the eight compatibility conditions of Eq. (23) along with the four boundary conditions as listed in Eqs. (21) and (22). The solvability condition for the resulting set of 12 equations for the twelve unknowns gives us transcendental equations in β whose solutions are then used to determine the natural frequencies and mode shapes of this cantilevered beam with an intermediate hollow section. For each β, the non-trivial solution for the twelve unknowns gives us the scalable desired mode-shape. Substitution of the resulting mode shapes in Eq. (17) which is then substituted in Eq. (16) followed by multiplication of the first two equations in Eq. (16) by ψ_{si}, and then integrating them from 0 to L, (while using the orthogonality property of the mode shapes), results in the following equations of motion:

$$\begin{aligned}
&\left(\sum_i \int_0^L \rho A_s \psi_{si}\psi_{si}dz\right)\ddot{q}_{ui} + \sum_i \frac{C_i}{L}\left(\int_0^L \psi_{si}\psi_{si}dz\right)\dot{q}_{ui} + \sum_i 2\Omega\left(\int_0^L \rho A_s \psi_{si}\psi_{si}dz\right)\dot{q}_{vi} - \\
&\sum_i \Omega^2\left(\int_0^L \rho A_s \psi_{si}\psi_{si}dz\right)q_{ui} - \sum_i\left(\int_0^L \rho I_s \psi_{si}\psi_{si}dz\right)\beta_{si}{}^2\ddot{q}_{ui} - \\
&\sum_i 2\left(\int_0^L \rho I_{ps}\psi_{si}\psi_{si}dz\right)\Omega\beta_{si}{}^2\dot{q}_{vi} + \sum_i\left(\int_0^L EI_s\psi_{si}\psi_{si}dx\right)\beta_{si}{}^4 q_{ui} + \\
&\left[k_d\left(\sum_j q_{uj}\psi_{sj} - u_d\right)\psi_{si} + c_d\left(\sum_j \dot{q}_{uj}\psi_{sj} - \frac{\partial u_d}{\partial t}\right)\psi_{si}\right]_{z=z_d} = f_{u3}(z_f,t)\psi_{si};\ i,j = 1,\ 2,\ \cdots\cdots
\end{aligned} \tag{24}$$

$$\begin{aligned}
&\sum_i\left(\int_0^L \rho A_s \psi_{si}\psi_{si}dz\right)\ddot{q}_{vi} + \sum_i \frac{C_i}{L}\left(\int_0^L \psi_{si}\psi_{si}dz\right)\dot{q}_{vi} + \sum_i 2\Omega\left(\int_0^L \rho A_s \psi_{si}\psi_{si}dz\right)\dot{q}_{ui} - \\
&\sum_i \Omega^2\left(\int_0^L \rho A_s \psi_{si}\psi_{si}dz\right)q_{vi} - \sum_i\left(\int_0^L \rho I_s \psi_{si}\psi_{si}dz\right)\beta_{si}{}^2\ddot{q}_{vi} + \\
&\sum_i 2\left(\int_0^L \rho I_{ps}\psi_{si}\psi_{si}dz\right)\Omega\beta_{si}{}^2\dot{q}_{ui} + \sum_i\left(\int_0^L EI_s\psi_{si}\psi_{si}dx\right)\beta_{si}{}^4 q_{vi} + \\
&\left[k_d\left(\sum_j q_{vj}\psi_{sj} - v_d\right)\psi_{si} + c_d\left(\sum_j \dot{q}_{vj}\psi_{sj} - \frac{\partial v_d}{\partial t}\right)\psi_{si}\right]_{z=z_d} = f_{v3}(z_f,t)\psi_{si};\ i,j = 1,\ 2,\cdots\cdots
\end{aligned} \tag{25}$$

$$\begin{aligned}
&m_d\left(\frac{\partial^2 u_d}{\partial t^2}\right) + 2m_d\Omega\left(\frac{\partial v_d}{\partial t}\right) - m_d\Omega^2 u_d \\
&+\left[k_d\left(u_d - \sum_j q_{uj}\psi_{sj}\right) + c_d\left(\frac{\partial u_d}{\partial t} - \sum_j \dot{q}_{uj}\psi_{sj}\right)\right]\delta(z - z_d) = 0;
\end{aligned} \tag{26}$$

$$\begin{aligned}
&m_d\left(\frac{\partial^2 v_d}{\partial t^2}\right) - 2m_d\Omega\left(\frac{\partial u_d}{\partial t}\right) - m_d\Omega^2 v_d \\
&+\left[k_d\left(v_d - \sum_j q_{vj}\psi_{sj}\right) + c_d\left(\frac{\partial v_d}{\partial t} - \sum_j \dot{q}_{vj}\psi_{sj}\right)\right]\delta(z - z_d) = 0.
\end{aligned} \tag{27}$$

For a single mode approximation, these four equations can be rewritten in a compact matrix form as:

$$([\mathrm{M}] + [\mathrm{M}]_R)\{\ddot{\mathrm{q}}\} + ([\mathrm{C}] + [\mathrm{C}]_{Co} + [\mathrm{C}]_G)\{\dot{\mathrm{q}}\} + ([\mathrm{K}] + [\mathrm{K}]_{Ce})\{\mathrm{q}\} = \{\mathrm{f}\} \tag{28}$$

wherein $\{\mathrm{q}\} = \{q_{ui},\ u_d, q_{vi},\ v_d\}^T$, $\{\mathrm{f}\} = \{f_{u3}\psi_{si}(z_f),\ 0, f_{v3}\psi_{si}(z_f),\ 0\}^T$, (wherein '$i$' in turn represents the mode number), $[\mathrm{M}]$ is the mass matrix, $[\mathrm{M}]_R$ is the rotational inertia matrix, $[\mathrm{C}]$ is the damping matrix, $[\mathrm{C}]_{Co}$ and $[\mathrm{C}]_G$ are the damping matrices to compute the Coriolis and Gyroscopic effects, respectively, $[\mathrm{K}]$ is the stiffness matrix, and $[\mathrm{K}]_{Ce}$ is the stiffness matrix to compute the centrifugal effect of the beam and the absorber.

Note that the presence of the absorber causes a coupling between the various modal coordinates and hence, a systematic study of the higher modes will necessarily require us to consider a multi-mode approximation even though we have written a single mode approximation above. However, for a study involving the first mode (which is the most flexible one and hence, of interest to this study), a single mode approximation as written above is justified. This modal coupling between the various modal coordinates due to the absorber might require a multi-mode analysis for better convergence. However, in this preliminary study on including the effect of

rotational speed on the tuning of the absorber, we have avoided a multi-mode approximation for simplicity of understanding. This simplicity also facilitates comparison of the results from this study with the classical Den-Hartog approach of tuning the absorber which is based on a single mode approximation.

Inclusion of the influence of the Coriolis, rotational inertia, gyroscopic and centrifugal effects of the holder and of the Coriolis and centrifugal effects of the absorber to develop a damped tooling system is a new and modest technical contribution to the literature in which prior work was limited to only considering the influence of gyroscopic effects in the design of damped milling tool holding systems.

To characterize the free vibration problem and to investigate how the dynamics of the tool holder with an absorber integrated within it change with speed, Eq. (28) can be solved for every speed of interest for the case of $\{f\} = \{0\}$, and the resulting imaginary parts of the complex-valued eigenvalues will help obtain a sense of how the eigenvalues (natural frequencies) change with speed.

To obtain the frequency response functions (FRFs), we assume that for a harmonic excitation, i.e., for $f_{u3}(t) = F_{u3}e^{j\omega t}$, $f_{v3}(t) = F_{v3}e^{j\omega t}$, the response too will be harmonic, i.e., $q_{ui}(t) = Q_{ui}e^{j\omega t}$, $q_{vi}(t) = Q_{vi}e^{j\omega t}$, $u_d(t) = U_d e^{j\omega t}$, $v_d(t) = V_d e^{j\omega t}$. The FRF matrix [H] hence becomes:

$$[\mathrm{H}] = [\mathrm{RM}]\left[\begin{array}{c}(-\omega^2)([\mathrm{M}] + [\mathrm{M}]_R) + (\mathrm{j}\omega)([\mathrm{C}] + [\mathrm{C}]_{Co} + [\mathrm{C}]_G) \\ +([\mathrm{K}] + [\mathrm{K}]_{Ce})\end{array}\right]^{-1}[\mathrm{FM}]$$

wherein,

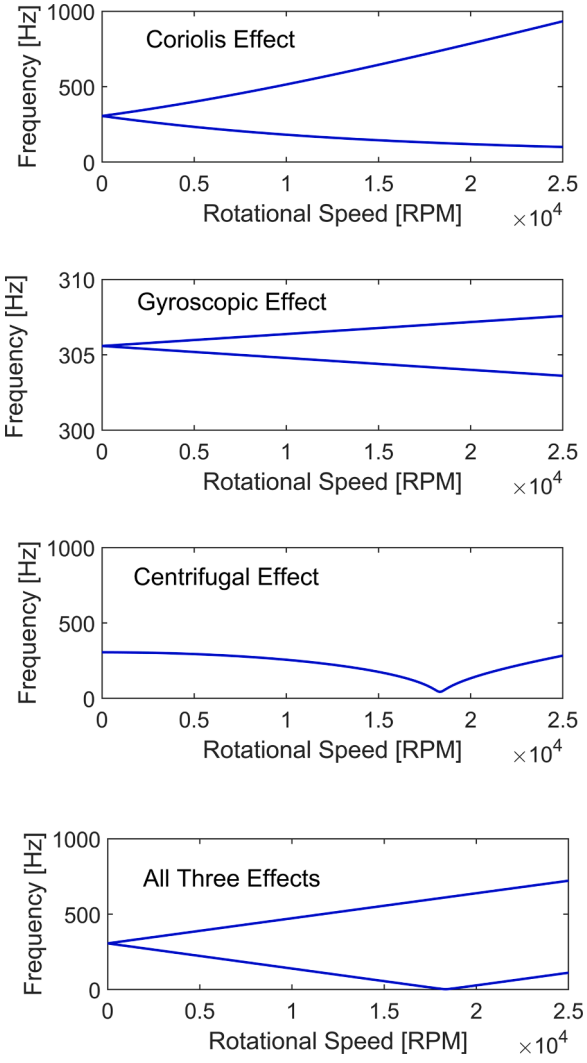

Fig. 2. Influence of the Coriolis, gyroscopic, centrifugal and combined effects on the speed-dependent tool holder dynamics characterized by natural frequencies.

$$[\mathrm{RM}] = \begin{bmatrix} \psi_s(z_r) & 0 & 0 & 0 \\ 0 & 1 & 0 & 0 \\ 0 & 0 & \psi_s(z_r) & 0 \\ 0 & 0 & 0 & 1 \end{bmatrix}, \quad [\mathrm{FM}] = \begin{bmatrix} \psi_s(z_f) & 0 & 0 & 0 \\ 0 & 0 & 0 & 0 \\ 0 & 0 & \psi_s(z_f) & 0 \\ 0 & 0 & 0 & 0 \end{bmatrix} \tag{29}$$

wherein $\psi_s(z_r)$ and $\psi_s(z_f)$ are the eigenvectors at the response and excitation locations, respectively. Solving Eq. (29) for a given speed and for the range of frequencies of interest, will result in the direct and cross speed dependent FRFs of the tool holding system with an absorber integrated within it.

Forced vibration response of the tool holder and/or the absorber ($\{q\}$), is obtained by assuming the time-periodic milling cutting forces acting at the free end can be approximated by a single harmonic excitation of the form of $f_{u3}(t) = F_{u3}e^{i\omega t}$ and/or $f_{v3}(t) = F_{v3}e^{i\omega t}$ in the x and the y directions, respectively. Eq. (28), in a slightly modified form can then be easily solved to obtain $\{q\}$ for different excitation frequencies (ω) of interest.

Furthermore, if the speed-dependent behavior of only the tool holder system without the absorber is of interest, the locally hollow cavity within the tool holder is neglected, and the holder is considered to be a solid beam. As such, the beam will have only one section, and will not be partitioned into three sections as was done to accommodate the absorber. The assumed mode shape in Eq. (18) will hence have only four unknowns that need to be identified by using the boundary conditions at the fixed and free end listed in Eqs. (21) and (22). Furthermore, since there is no absorber, Eqs. (26) and (27) can be neglected, and the resulting simplified forms of Eqs. (28) and (29) can be similarly solved to obtain the speed-dependent dynamics and/or the speed-dependent FRFs of only the tool holder. This is presented in the next section to better appreciate the effect of the rotational spped on the dynamics of the tool holding system and motivate the optimization problem for the tuning of the absorber that will be set up in Section 4.

3. Speed-dependent dynamics of the milling tool holding system without the absorber

This section discusses how the dynamics characterized by natural frequencies and by the FRFs of the tool holder at the cutting point change with speed. All analysis herein is for the case of the tool without the absorber. The tool holder is assumed to be made of steel with its density being $\rho = 7850$ kg/m^3, and its modulus of elasticity being $E = 200$ GPa. The tool holder is assumed to have a diameter $D = 50$ mm, and its length L from the gage plane is assumed to be 340 mm. This length includes a face mill of length $L_r = 40$ mm. Hence, the overall slenderness (L/D) ratio of the tool holding system is ~7. Damping of the holder is assumed to be of the form of $C_i = 2\zeta_0 M_i \omega_{ni}^2/\omega$, wherein M_i is the modal mass of the i^{th} natural frequency ω_{ni}, ω is the excitation frequency, and the damping ratio, ζ_0 is assumed to be 1%.

3.1. Influence of the rotational speed on dynamics of the milling holder

Dynamics characterized by natural frequencies changingwith rotational speed are shown in Fig. 2. Results in Fig. 2 are limited to characterizing only the dynamics of the tool represented by its first fundamental bending mode. Since the fundamental bending mode of the tool holding system is much more flexible than the higher frequency modes [35], all analysis herein is limited to only the first fundamental mode. To characterize how each of the Coriolis, gyroscopic, and centrifugal effects contribute differently to the change in the dynamics, Fig. 2 shows the results for when each of these effects is considered individually, and also for the case when all effects were considered together. Influence of select rotational effects were obtained by neglecting appropriate terms from the equations of motion listed in Eqs. (24) and (25). Since rotational inertia is independent of speed (see Eq. (15)), it is not shown in Fig. 2.

In general, it is evident from Fig. 2 that the Coriolis, centrifugal, and gyroscopic effects all appear to contribute differently to the change in the dynamics. The gyroscopic effects have less of an influence on the speed-dependent dynamics as compared with the Coriolis and centrifugal effects. These observations are consistent with other related findings [30,31]. The centrifugal effect decreases the natural frequency, and does not split the mode into two, whereas because the Coriolis effects couple the two orthogonal directions in the rotational frame (see Eqs. (24) and (25)), the mode splits and there is a corresponding forward and backward mode each for any non-zero speed. The Gyroscopic effect also splits the mode into forward and backward modes but the change in frequency corresponding to both modes is insignificant compared to the Coriolis effect. The first critical speed, i.e., the speed at which a natural frequency corresponding to a backward wave becomes zero, corresponding to the first mode occurs at ~18,270 RPM.

The tool holding system of interest is designed to support medium sized face mills which can be used to cut many different materials. Since the expected cutting speeds (V_c) are not likely to exceed 1000 m/min (even for the case of cutting Aluminum), the maximum speed that the tool holder will rotate at will be ~6000 RPM ($V_c = \pi DN$). This speed is well below the first critical speed. Critical speed related instabilities are hence not of interest to us, and we are concerned only with how the dynamics change with speed.

For the speed range of interest, i.e., up to a speed of ~6000 RPM, the natural frequency of the first mode changes from 306 Hz at the zero speed to 206 Hz for the backward wave, and to 406 Hz for the forward wave, i.e., a change of ~33%. These changes are not insignificant. Since the known methods [13,15–21] of tuning absorbers for tooling systems assume that the dynamics of the primary system do not change, those methods will clearly be inadequate. Moreover, most classical methods [13,15–19] of tuning assume that the primary system's dynamics can be described by a single degree of freedom system. As such, tuning is then about finding the optimal ratios of frequencies and masses between the secondary and the primary systems. However, when every zero-speed mode splits in two for all non-zero speeds, there is no unique 'optimal' frequency and mass ratio. Hence the classical methods of tuning are clearly not appropriate in the case of systems with speed-dependent characteristics. Tuning an absorber for applications in tooling systems when there are multiple modes in the primary system and with each of those modes changing their character with speed, remains

unaddressed yet, and will be appropriately addressed in this paper.

All analysis herein was limited to characterizing how the natural frequencies are speed-dependent. Though important, the change in natural frequencies does not directly govern the machining stability of the system, which is governed by the dynamics characterized by FRFs [37,38]. To get a sense of how the chatter-free stability of the milling tool holding system changes with speed, the change in FRFs with speed are characterized next.

3.2. Influence of the rotational speed on the FRFs of the milling holder

Dynamics characterized by FRFs changing with speed are shown in Fig. 3. As representative examples of how the FRFs change with speed, results in Fig. 3 are shown for the zero speed case along with FRFs evaluated at speed intervals of 1000 RPM, and up to a speed of 6000 RPM – which is the maximum speed of interest. And, even though the FRFs are complex valued, Fig. 3 only shows their magnitudes changing with speed. FRFs shown in Fig. 3 include the direct and cross FRFs evaluated at the cutting end. Since we assume the beam to be symmetric about its central axis, the direct *x* and *y* directional FRFs are the same, and the cross *xy* and *yx* directional FRFs are also the same.

Changes in frequencies of the split modes observed in Fig. 3 are like those observed in Fig. 2. Also evident from Fig. 3 is that at zero speeds the cross FRFs are zero, and at any non-zero speed, the magnitude of the cross FRFs are almost the same as the direct FRFs at that speed. The cross FRFs becoming dominant at non-zero speeds are due to the Coriolis and the gyroscopic effects coupling the vibrations in orthogonal planes. Since cross FRFs also govern the chatter-free milling stability limits [37,38], factoring their speed-dependent characteristics in the design of damped tooling systems is important. Though important, this aspect remains unaddressed yet, and will be discussed in Section 4.

4. The optimization problem

Since the damped milling tool holding system is being designed to make possible chatter-free machining, the maximization of the chatter-free stability limit is treated as the objective function. The stability model used to estimate the chatter-free stability limit is first discussed herein, followed by describing the optimization problem that accounts for the speed-dependent dynamics of the tool holding system.

4.1. Milling stability model

Though there exist very many high-fidelity milling stability models, since the frequency domain model [37] is fairly accurate and computationally inexpensive, it facilitates the optimization investigations, and is hence preferred herein. As per the model, the stability of a milling system is determined using a modal model of the machine/tool and the following characteristic equation:

$$\det([\mathrm{I}] + \Lambda[\mathrm{H}_{or}]) = 0, \tag{30}$$

wherein, $\Lambda = -\frac{N_t}{4\pi}\, aK_{tc}(1 - e^{-j\omega_c \tau})$, and wherein Λ is the eigenvalue of the characteristic equation, N_t are the number of teeth on the

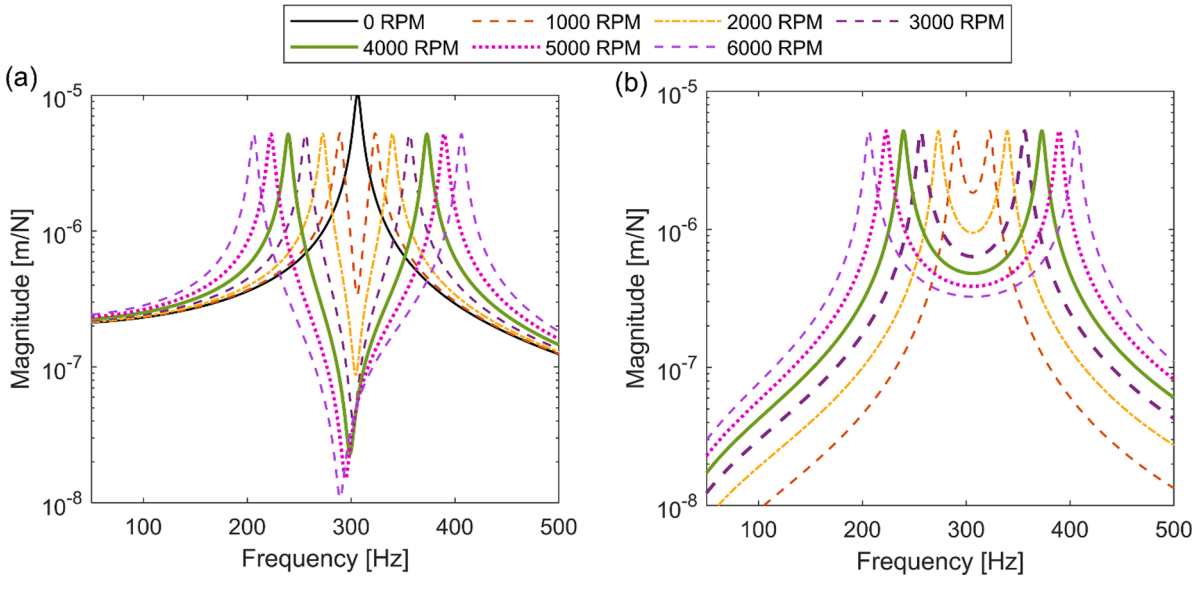

Fig. 3. Influence of the rotational speed on the FRFs of the milling holder. (a) Direct FRFs, (b) Cross FRFs.

cutter, K_{tc} is the cutting force coefficient of the material being cut, a is the axial depth of cut, ω_c is the chatter frequency, and, τ is the tooth passing period. The oriented directional matrix $[\mathrm{H}_{or}]$ within Eq. (30) is expressed as:

$$[\mathrm{H}_{or}] = \begin{bmatrix} \alpha_{xx} & \alpha_{xy} \\ \alpha_{yx} & \alpha_{yy} \end{bmatrix} \begin{bmatrix} h_{xx}(\omega_c) & h_{xy}(\omega_c) \\ h_{yx}(\omega_c) & h_{yy}(\omega_c) \end{bmatrix}, \tag{31}$$

wherein α_{xx}, α_{xy}, α_{yx}, and α_{yy} are the averaged directional coefficients which depend on the radial engagement conditions of the tool with the workpiece, and on the cutting coefficients of the material being cut, and these can be determined as described in [38]. The FRFs h_{xx}, h_{xy}, h_{yx}, and h_{yy} are obtained by solving Eq. (29).

Since maximizing the absolute chatter-free depth of cut is of interest to us, that critical limit, which is governed by the parameters in Eq. (30) and Eq. (31), can be analytically shown to be [38]:

$$a_{\mathrm{lim}} = -\frac{2\pi \mathrm{Re}(\Lambda)}{N_t K_{tc}} \left(1 + \left(\frac{\mathrm{Im}(\Lambda)}{\mathrm{Re}(\Lambda)}\right)^2\right), \tag{32}$$

wherein $\mathrm{Re}(\Lambda)$ and $\mathrm{Im}(\Lambda)$ are the real and imaginary parts of the eigenvalue of the characteristic equation.

4.2. Maximizing chatter-free stability limit by tuning the absorber

The optimization problem is setup to find the equivalent stiffness (k_d) and damping (c_d) of the absorber for a given absorber mass (m_d) that maximizes the chatter-free stability limit over the range of speeds of interest. The objective function is hence defined as:

$$\begin{aligned} &\text{maximize } f_{\mathrm{obj}}(k_d, c_d) = \sqrt{\frac{\sum_{r=1}^{r=n} a_{\mathrm{lim}}(\Omega_r, m_d)}{n}} \\ &\text{subject to : } 5 \times 10^4 < k_d < 5 \times 10^7;\ 10 < c_d < 1200. \end{aligned} \tag{33}$$

wherein n is the total number of rotational speeds Ω_r that the absorber must be tuned for, and k_d and c_d are the stiffness and damping coefficients of the absorber, and bounds on it are taken from results in [21]. To maximize the objective function in Eq. (33) we prefer to use the Nedler-Mead algorithm [39]. For investigations herein, the initial guess for the absorber's stiffness and damping coefficient is taken to be 5×10^5 N/m and 100 N-s/m, respectively.

Since the damped tooling system of interest may be used to cut at any speed up to 6000 rpm, no weights are assigned for speeds during optimization. However, since the methodology is generalized, and if the damped tooling system is to be designed for specific cutting speed regimes, weights can easily be added to those speeds during the optimization procedure.

For the absorber to be effective, it is expected to typically vibrate with amplitudes larger than the holder (at the absorber mounting location) such as to dissipate energy. Since the gap between the absorber and the holder is assumed to be fixed, for every combination of the optimized parameters, we check if there is any likelihood of the absorber impacting the holder. Since impacts may potentially destabilize the system, if the relative amplitudes of vibrations of the absorber and of the tool holder, i.e., $u|_{z_d} - u_d$, and/or $v|_{z_d} - v_d$ equals the gap, or is greater than the gap, those absorber parameters are suitably rejected from being potential 'optimal' candidates, and the search procedure is continued.

5. Results and discussion

For analysis herein, the tool holder is assumed to have the same specifications as described in Section 3, i.e., the holder has a diameter of 50 mm, and its slenderness ratio is ~7, which includes a face mill of 50 mm diameter and length of 40 mm. The face mill is assumed to have five teeth, i.e., $N_t = 5$, and it is assumed to be cutting Aluminium. Two cutting conditions are considered. In one case, cutting takes place in an up-milling mode with 50% radial engagement, and in the other case, slot milling is taking place with a 100% engagement of the tool with the workpiece. For all investigations herein, the radial and tangential cutting coefficients for Aluminium are assumed to be 200 and 800 MPa, respectively.

The absorber integrated within the holder is assumed to be fixed at a distance of 227 mm from the fixed end. Moving the absorber any closer to the free end is constrained by the practical considerations of the holder supporting a face mill mounted on an adaptor (see Fig. 1). The local cavity within the holder to house the absorber is assumed to be of a diameter of 25 mm and of a length of 110 mm (i.e., $a = 172$ mm and $b = 282$ mm – see Fig. 1). And, even though the absorber is modelled as a lumped mass, it is assumed to have a diameter of 23 mm and a length of 100 mm. This makes for a 1 mm radial gap between the absorber and the hollow cavity in the holder. Since the size of the absorber is fixed, its mass may be varied by choosing materials of different densities.

With the specifications described above, we first characterize how the optimized stiffness and damping vary with changing mass of the absorber. We also discuss how the maximized chatter-free stability changes with these parameters. This is followed by evaluating the speed-dependent dynamics of the tool holder integrated with a tuned absorber with fixed parameters. Finally, we present the stability characteristics of the optimally tuned and damped rotating milling tool holding system. We also present representative checks ensuring that the relative forced vibration response of the tool holder and the absorber combine is always less than the gap between the absorber and the holder. To contextualize our findings, where possible, we also contrast results obtained with procedures outlined herein with those obtained using the classical methods of tuning absorbers that do not account for the speed-varying characteristics of

the primary system.

5.1. Dependence of the maximized chatter-free stability limit on the absorber's parameters

The maximized chatter-free depths of cut for different combinations of mass, stiffness, and damping of the absorber for the two different cutting conditions are summarized in Fig. 4. The figure also characterizes how the optimized stiffness and damping of the absorber change for different assumed values of its mass.The optimization problem evaluates the limiting depth of cut at discrete speeds, which in turn are based on evaluation of the dynamics of the tool holding system at those same discrete speeds. We hence assume that the speed range from 0 – 6000 RPM can be sufficiently described by 12 steps (i.e., $n = 12$) with step sizes of 500 RPM.

To contextualize our findings, Fig. 4 also shows the results obtained from Den Hartog's [15] classical method of tuning absorbers that suggests the optimal frequency and mass ratios as the ratios of the natural frequencies and the masses of the secondary and primary systems, respectively. As per [15], the optimal frequency ratio is given by: $\frac{1}{1+\mu}$, and the optimal damping ratio is given by: $\sqrt{\frac{3\mu}{8(1+\mu)}}$, wherein μ is the mass ratio. Seeing how the optimal frequency and damping ratios are mass ratio dependent, evaluation of the

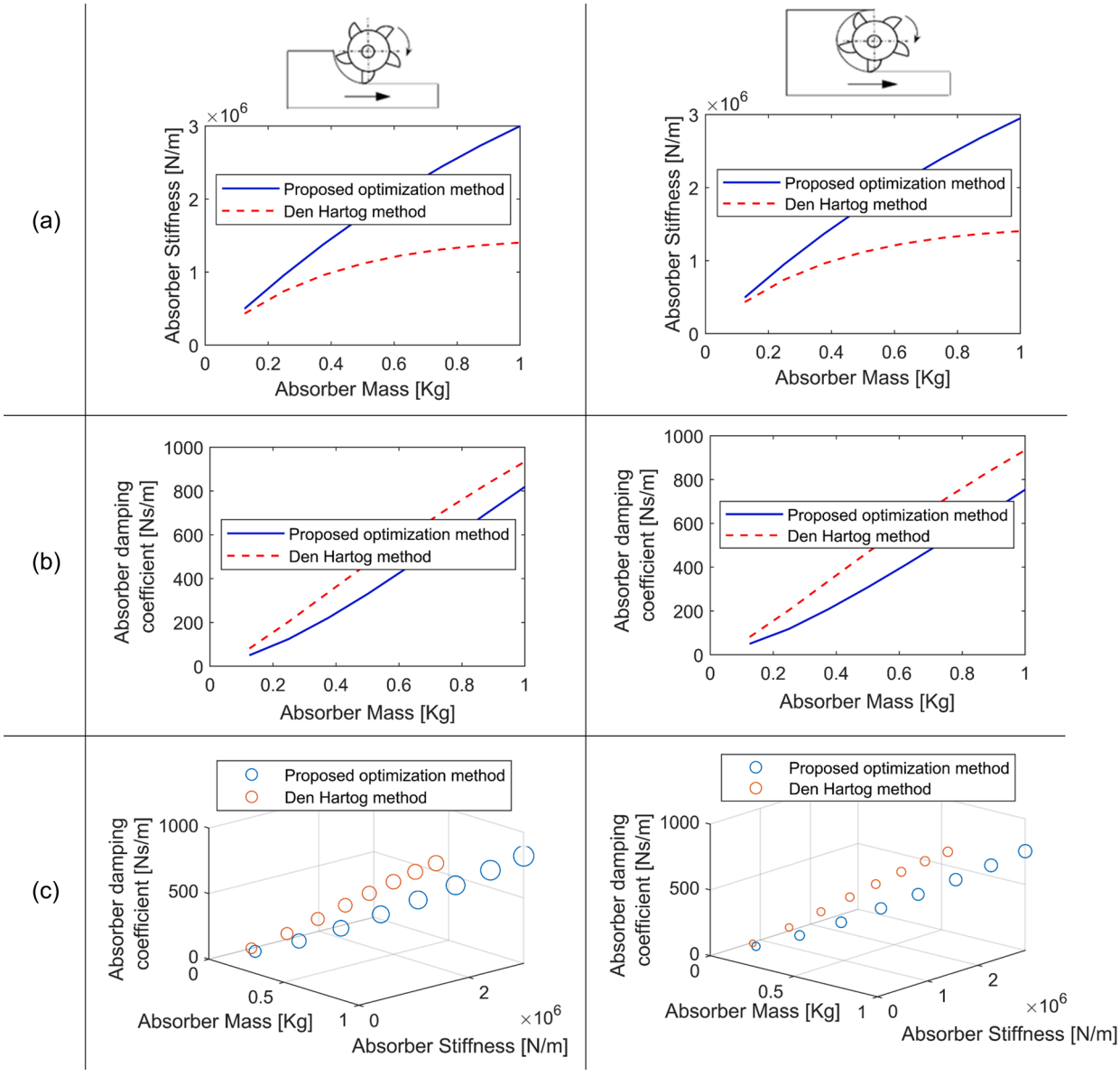

Fig. 4. Optimized results for cutting of Aluminium in the 50% up-milling (left column) and in the slot-milling mode (right column), (a) Optimized stiffness of the absorber changing with the absorber's mass, (b) Optimized damping of the absorber changing with the absorber's mass, (c) Maximized chatter-free depths of cut changing with the absorber's mass, stiffness, and damping.

modal mass of the primary system is essential. However, since the dynamics of the tool holding system are speed-dependent, and since each mode splits into two at every non-zero speed, the modal mass of each mode becomes speed-dependent. Furthermore, since there are two modes in the direct FRF and two also in cross FRF, and each of these changes their characteristics with speed, selection of the modal mass from FRFs is non-trivial. Hence, the modal mass for use in the Den Hartog's method is instead taken to be the modal mass at the zero-speed. Since the zero-speed direct FRF has only one mode, and since the cross FRF is zero at the zero-speed, the modal mass of the primary system is determined from the direct FRF. The modal mass can be evaluated using any one of the standard modal identification techniques [42], and it is found to be 1.4146 kg.

As is evident from Fig. 4 (a-b), the optimum stiffness and damping characteristics of the absorber increase with an increase in the mass of the absorber for the proposed method as well as for the Den Hartog's method, and that the relationships are weakly nonlinear. Also evident from Fig. 4(a-b) is that the increase in the stiffness and damping characteristics obtained with the proposed approach do not appear to be strongly dependent on the engagement conditions. Furthermore, and interestingly, for a given absorber mass, the optimized stiffness found using the proposed approach is always higher than that predicted using Den Hartog's method. And, though optimized damping obtained using Hartog's method is always more than the proposed method, the differences are not as stark as in the case of stiffness.

The difference in the maximized chatter-free depths of cut for the two different methods to optimize the absorber's parameters is shown in Fig. 4(c), wherein the size of the circles correspond to the possible chatter-free depths of cut. Since stable depths of cuts are

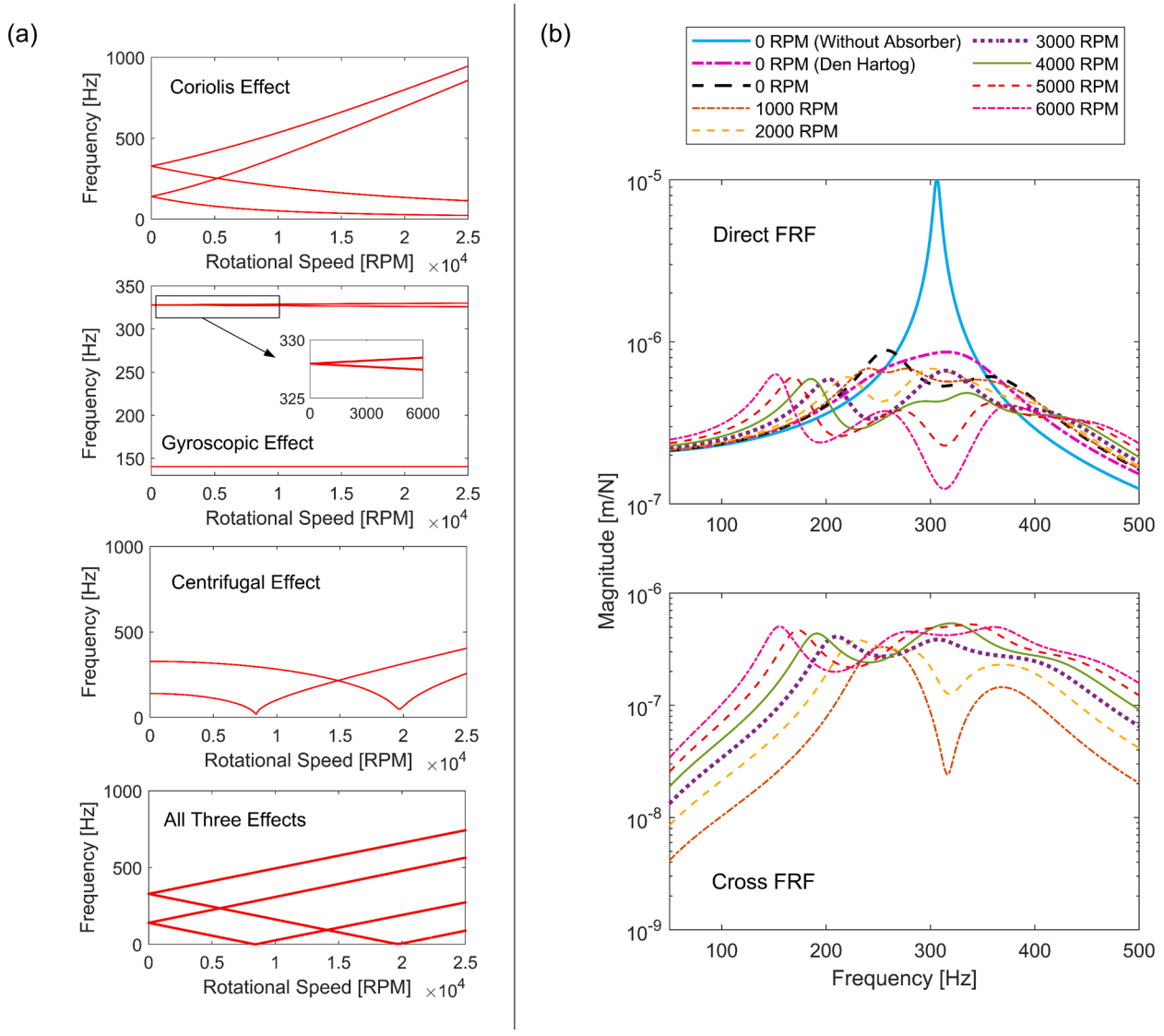

Fig. 5. (a) Influence of the Coriolis, gyroscopic, centrifugal and combined effects on the speed-dependent tool holder with absorber dynamics characterized by natural frequencies, (b) Influence of speed on the direct and cross FRFs of the milling tool holder with the absorber along with the speed-independent FRF of the holder without the absorber.

inversely proportional to the engagement conditions, the chatter-free axial depths for the 50% up-milling engagement conditions are higher than the case of slot milling. Also evident from Fig. 4(c) is that the possible depths of cuts obtained with the proposed method are always higher than the results obtained using Den Hartog's method. This suggests that if absorbers are tuned to respect the speed-dependent dynamics of the primary system, then a better design for chatter-resistant milling tooling systems is possible. Moreover, since the proposed method does not result in analytical relationships between frequency, damping and mass ratios as with Den Hartog's method, those relationships are deducible from results shown in Fig. 4, i.e., the results in the figure suggest what the absorber stiffness and damping should be for a given mass of the absorber.

Based on the results in Fig. 4, it can be concluded that the chatter-free depth of cut increases with an increase in the absorber's mass, stiffness, and in its damping. Since the stiffness and damping characteristics of the absorber are not known a priori, and largely depend on the elastomeric properties of the O-rings supporting the absorber, it is clear that a stiffer O-ring with higher damping will be favourable. Since O-rings are complex elastomers that may have different stiffness and damping characteristics in tension/compression, in torsion, and in shear, and since these materials exhibit frequency-dependent nonlinearities, selecting/designing/identifying materials with appropriate stiffness and damping characteristics is not trivial. And, since the damping performance of tooling systems is governed by stiffness and damping characteristics of O-rings, selecting/designing/identifying the appropriate material is paramount.

If O-rings are to be selected from those that are available commercially and whose stiffness and damping characteristics are not known a priori, O-rings with different materials may be tried to investigate their influence on the damped response of the tooling system before deciding on the appropriate material, as was done in [13]. However, such a try-and-see approach could become cumbersome, since every time the O-rings are tuned, experiments may need to be repeated to get a sense of the comparative behavior of different materials. Alternatively, it is possible to identify its stiffness and damping characteristics using the 'inverse receptance procedure' in which parameters are identified from the measured receptance of the assembled damped tool and from the measured/modelled rigid body receptance of the absorber mass, as was done in [21]. This method can also be used to compare behavior of O-rings made of different materials. However, the approach too has limitations due to point coupling approximations. The method is also sensitive to measurement noise. Moreover, for every tuning setting, stiffness and damping characteristics will need to be identified afresh. It is also possible to design O-ring materials with desired, model-predicted optimal stiffness and damping characteristics. Design performance can be evaluated using 'dynamic mechanical analyzers', and if found appropriate those values can be used in models to predict the expected assembled damped system response.

Since in the investigations herein, the size of the absorber and of the cavity it is housed in is fixed, to select an absorber with a higher mass, materials with higher density can be chosen. If on the other hand, the size of the hollow cavity within the holder and that of the absorber can also be changed, a change in absorber size along with a change in material can both bring about a change in the mass of the absorber, as desired. These results are hence useful to guide the design and development of damped tooling systems.

5.2. *Speed-varying characteristics of an optimally tuned and damped milling tool holding system*

Since our results suggest selecting an absorber with a higher mass, results herein are presented for an absorber having a mass of 0.62 kg. Since the size of the absorber is assumed fixed, this mass corresponds to an absorber made of tungsten carbide that has density of ~15,000 kg/m^3. We choose tungsten carbide since it is the preferred material for tuned mass dampers integrated within tooling systems [18,21]. The optimized stiffness and damping of the absorber for this mass was selected from the results in Fig. 4, and are $k_d = 2.1 \times 10^6$ N/m and $c_d = 444$ N-s/m, respectively. The speed-varying characteristics of the tool holder integrated with this absorber are shown in Fig. 5, which also includes the speed-varying characteristics of only the tool holder (same as in Section 3).

Natural frequencies changing with speeds are shown in Fig. 5(a), and the FRFs changing over the range of speeds of interest are shown in Fig. 5(b). Fig. 5(b) also shows the zero-speed FRFs for the damped tool as well as for the tool without the absorber, and the FRF obtained using the Den Hartog's method of tuning the absorber. Since Den Hartog's method is not suitable to investigate the speed-dependent dynamics, FRFs with it are limited to only the zero-speed case. Results in Fig. 5 are obtained by solving Eqs. (28 and 29), and hence they are independent of the cutting conditions.

As is evident from Fig. 5(a), the absorber has the additional effect of the splitting the modes, i.e., in addition to the splitting due to the rotational effects such that for every speed there are now two modes, with their separate forward and backward components. This is evident from the speed-dependnet natural frequencies in Fig. 5(a), and the from the FRFs in Fig. 5(b). Also evident from Fig. 5(a) is that the zero-speed natural frequency of the first mode of the holder with an optimally tuned absorber is lower than the zero-speed natural frequency of the tool holder without the absorber. Also evident is that for the holder with the absorber, there are two critical speeds. The first of which occurs at ~8400 RPM. This has reduced from it being ~18,270 RPM for the tool holder without an absorber. And, even though the critical speed reduces, it is still higher than our speed range of interest. The reduction in the natural frequency and critical speed of the fundamental mode for the holder with the absorber is likely due to the added mass of the absorber.

Interestingly, even for the case of the tool holder with an optimally tuned absorber, the centrifugal effects have more of an influence on the speed-dependent dynamic behavior than the Coriolis and/or the gyroscopic effects. Though the gyroscopic effect splits the beam's mode, for the case of the absorber's mode, since only Coriolis and centrifugal effects were considered in the model, no splitting is observed.

Moreover, as is evident from the direct FRFs in Fig. 5(b), at zero-speeds, the peak magnitude of the flexible mode of the damped tool holder is reduced by ~92% in comparison to the tool holder without the absorber. This level of reduction is like that achieved by tuning the absorber using Den Hartog's method – for which case, the optimal frequency and damping ratios are found from the known mass ratio. Also evident from the direct FRFs in Fig. 5(b) is how the magnitude of each of the non-zero speed mode(s) is lesser than the peak

magnitudes of the zero-speed mode(s). Also evident is how for the case of the cross FRFs, the magnitude of the most flexible peak tends to increase with speed.

5.3. Chatter-free speed-dependent characteristics

Stability behavior changing with speed is described herein. Since Eq. (32) only accounts for limiting depth of cut, influence of speed is accounted for as described in [38]. Predictions for the proposed approach are made with the same optimally tuned absorber parameters as those listed in Section 5.2. The resulting stability behavior for the case of up-milling with 50% engagement, and for the case of slot milling is shown in Fig. 6. To contextualize our results, Fig. 6 also includes stability behavior obtained with the dynamics of the tool holder without the absorber – for which case, only its zero-speed behavior is considered. Additionally, Fig. 6 also includes stability behavior obtained with the zero-speed dynamics of the tool holder integrated with the optimally tuned absorber using the proposed approach. To make comparisons furthermore meaningful, Fig. 6 also includes results obtained with Den Hartog's method of tuning the absorber integrated within the tool holder. Results in Fig. 6 are limited to the speed range of interest.

For the case of the holder integrated with an optimally tuned absorber, for every non-zero speed, the direct and cross FRFs are characterized by multiple modes, as shown in Fig. 5. With these speed-dependent dynamics, if, for example, the stability lobes were to be obtained using the speed-dependent behavior evaluated at a given speed, then, there would be multiple lobes corresponding to each mode in the FRF for that speed. The resulting continuous speed-dependent boundary between stable/unstable depths would be obtained from a convolution of these multiple lobes. Since dynamics change with speed, constructing such stability lobes for the case of

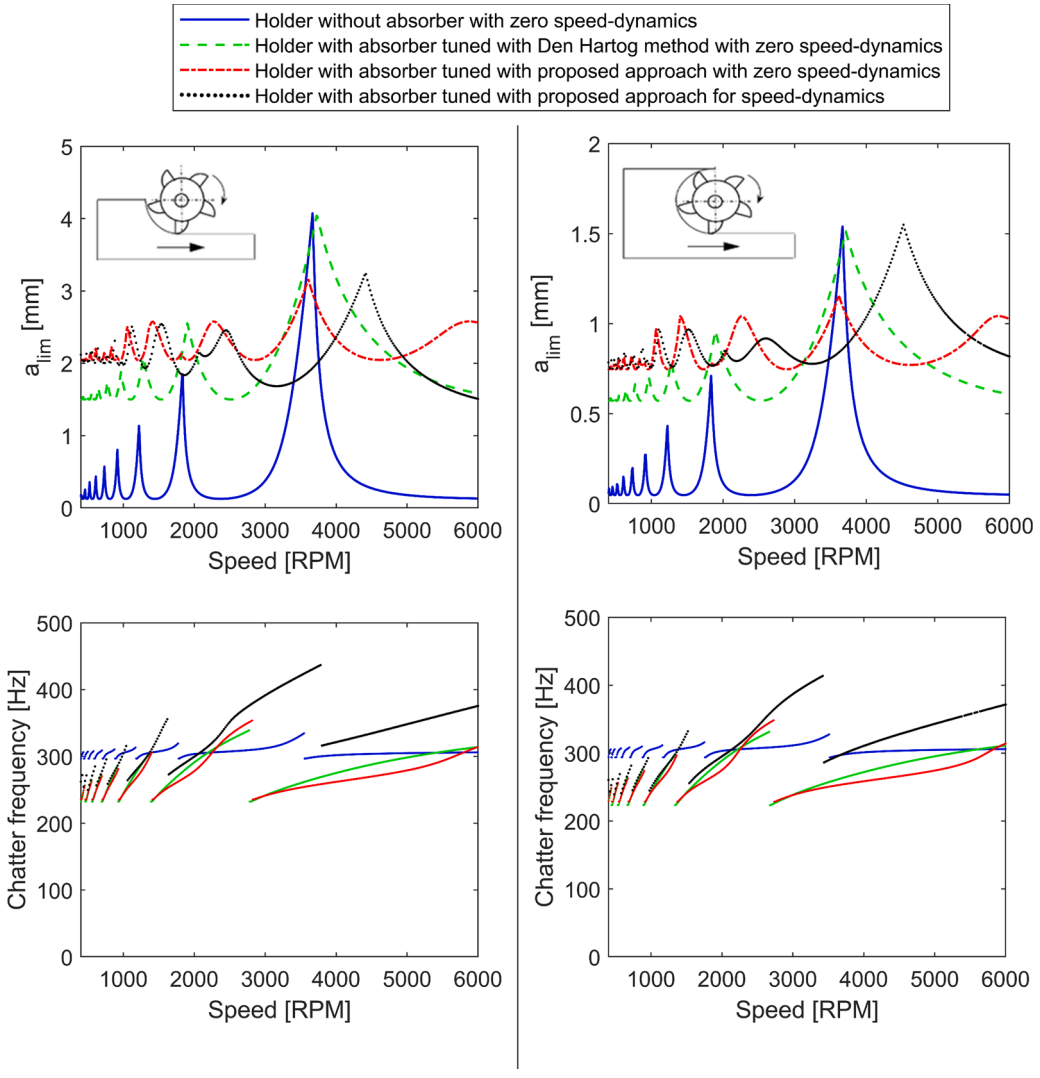

Fig. 6. Stability characteristics for the case of cutting with 50% engagement in the up-milling mode (left column) and in the slot milling mode (right column).

FRFs changing for every speed result in altogether different boundaries. And a global convolution of these multiple boundaries results in the speed-dependent stability behavior shown in Fig. 6.

As is evident from Fig. 6, for the case of up-milling with 50% radial immersion, the minimum chatter free-stability limit for cutting with a holder without an absorber is 0.12 mm. Whereas for the case of the holder with an optimally tuned absorber, the chatter limit evaluated using the zero-speed dynamics of the system is 2.1 mm, a significant ~1650% improvement, even when speed-dependent dynamics are not accounted for. For the case of the tuning using Den Hartog's methods, the improvement in the critical stable depth of cut over the case of a holder without the absorber is ~1150%. Though this is also a significant improvement, it is still less than the case of the holder tuned using the proposed approach. For stability evaluated with the tuned and damped holder's dynamics changing with speed, the gains over the case of cutting with a holder without a damper are evidently speed-dependent, yet significant, and almost always greater than the case of using Den Hartog's method of tuning.

Improvements in stability behavior for cutting in the slot milling mode are like those observed for up-milling with 50% engagement. In the slot milling mode, the minimum stable depth of cut for the holder without an absorber improves from 0.047 mm to ~0.78 mm for the holder with an optimally tuned absorber using the proposed approach.

The shift in the stability pockets observed in Fig. 6 are due to the dynamics being different with each method of tuning. As is also evident from Fig. 6, chatter frequencies for tuning the absorber using the proposed method that accounts for the speed-dependent dynamics are consistently higher than the chatter frequencies of the absorber tuned using the zero-speed dynamics. These observations are consistent with how the dynamics were observed to be speed-dependent in Fig. 3 and in Fig. 5.

5.4. Check for relative forced vibrations levels being less than the gap

Results herein discuss representative checks to ensure that the relative forced vibration response of the tool holder and the absorber combined is always less than the 1 mm gap between the absorber and the holder. Results herein are obtained with the same optimized absorber parameters that were used to generate results in Sections 5.2 and 5.3. To check the relative forced vibration levels, harmonic forces of the form of $200\cos\omega t$ were applied at the free end of the tool, wherein ω, the excitation frequency was varied such that the tooth passing frequencies, f_t ($=\frac{\Omega . N_t}{60}$ Hz) ranged from 50 to 500 Hz. Since the maximum speed of interest is 6000 RPM, and since there are five teeth on the cutter, the highest tooth passing frequency corresponds to 500 Hz. The force magnitude of 200 N corresponds to the maximum in-plane peak force for cutting with a feed/tooth of 0.1 with an axial depth of cut of 2 mm for the case of cutting in the 50% up-milling mode. This axial depth of cut lies just below the stability boundary shown in Fig. 6.

Since forces act on the cutting end, and since we are only concerned with the response of the holder at the absorber mounting

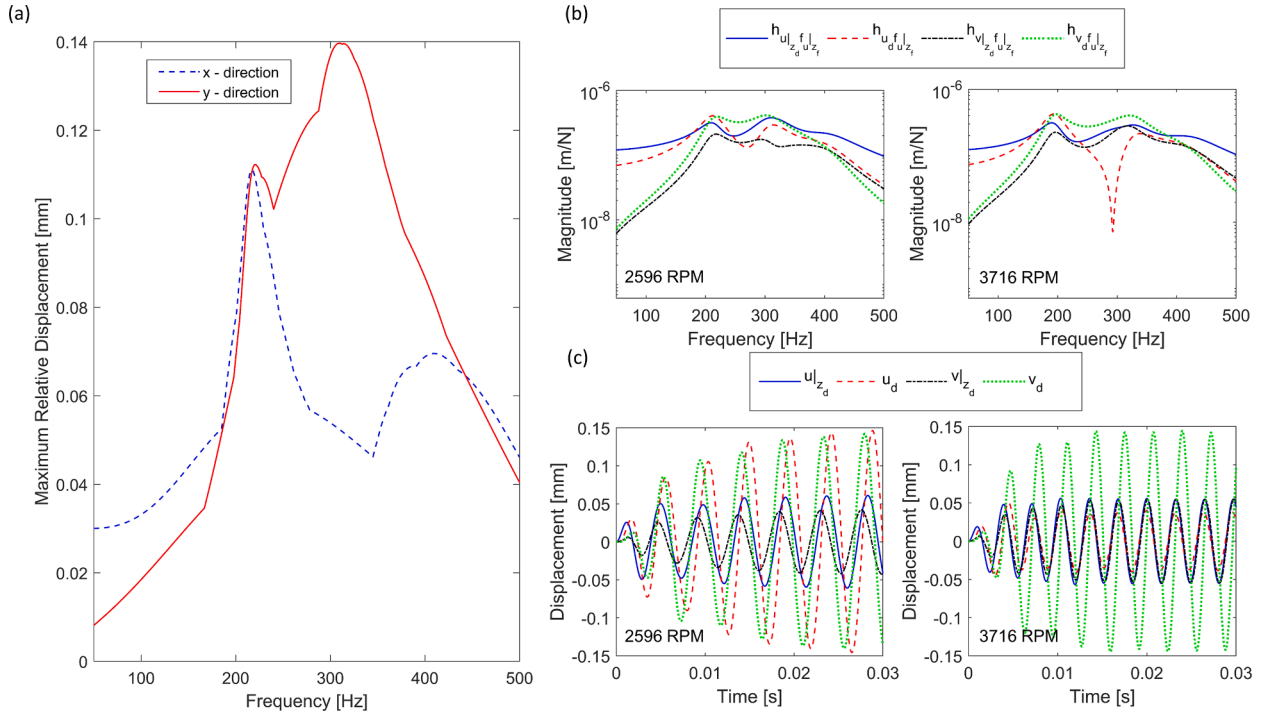

Fig. 7. (a) Maximum of the relative forced vibration levels between the holder and the absorber changing with tooth passing frequencies, (b) Representative cross FRFs between excitation at the free end of the tool holder and response at the absorber mounting location and at the absorber, (c) Representative examples of forced vibration response of the tool holder and of the absorber at different tooth passing frequencies (rotational speeds).

location ($u|_{z_d}$, $v|_{z_d}$), at first, the cross FRFs between these locations are obtained from Eq. (29). Since the response of the absorber in both orthogonal directions (u_d, v_d) is also of interest, the cross FRFs between the free end of the holder and the absorber are also obtained solving the same set of equations. Furthermore, since the rotational effects couple vibrations in orthogonal planes, we also evaluate those speed-dependent cross-directional FRFs, i.e., between excitation in the x direction, and response in the y direction. All these FRFs are used to then estimate the relative forced vibration response, i.e., to estimate $u|_{z_d} - u_d$, and $v|_{z_d} - v_d$.

The relative forced vibration response levels changing with tooth passing frequencies thus obtained are summarized in Fig. 7. These results were obtained by solving a slightly modified form of Eq. (28) by assuming an initial displacement and velocity are zero. Fig. 7(a) shows the maximum of the relative vibrations in either of the directions, i.e., $\max(u|_{z_d} - u_d)$ and $\max(v|_{z_d} - v_d)$. And, as is evident, the maximum of the relative vibrations in the x direction occur at the tooth passing frequency of 216.4 Hz. This corresponds to a spindle speed of ~2596 RPM. And, the maximum of the relative vibrations in the y direction occur at the tooth passing frequency of 309.7 Hz, which corresponds to a spindle speed of ~3716 RPM. Even at their maximum levels, the relative forced vibration response of the tool holder and the absorber combine are always less than the 1 mm gap between the absorber and the hollow cavity within the holder.

The cross FRFs at the tooth passing frequencies that result in the maximum forced vibration levels are shown in Fig. 7(b), and the corresponding response of the tool holder at the absorber mounting location and that of the absorber are shown in Fig. 7(c). In Fig. 7(b), $h_{u|_{z_d} f_u|_{z_f}}$ and $h_{v|_{z_d} f_u|_{z_f}}$ corresponds to the cross FRF between excitation at the free end of the tool in the x direction and response evaluated at the absorber mounting location within the holder in the x and in the y directions, respectively. The other cross FRFs in Fig. 7(b), i.e., $h_{u_d f_u|_{z_f}}$ and $h_{v_d f_u|_{z_f}}$ corresponds to the cross FRF between excitation at the free end of the tool in the x direction and response of the absorber in the x and in the y directions, respectively.

From Fig. 7(b) it is evident that the flexibility of the response of the absorber in the y direction increases with speeds due to the rotational effects coupling vibrations in orthogonal directions. Also evident from Fig. 7(b), is that the response of the absorber, is in general, more flexible than the response of the tool holder at the location where the absorber is attached with the tool holder in each direction. This suggests that vibrations are indeed transferred from the tool holder to the absorber, and the absorber dissipates that energy. This is also confirmed from the forced vibration response comparisons in Fig. 7(c). Also evident from Fig. 7(c) is that the amplitude of the response of the tool holder at the absorber mounting location is less than that of the absorber's in both directions of interest. This confirms that for an absorber with these optimized parameters, there will be no collision between it and the tool holder that could potentially destabilize the system.

6. Conclusion

This paper addressed tuning of absorbers integrated within rotating milling tool holding systems while accounting for their dynamics changing with speed – something that was unaddressed previously. The milling tool holder was modelled as a damped and cantilevered Euler-Bernoulli beam, and the absorber was integrated within the beam. The governing equations of motion of the beam and the absorber were derived by accounting for the gyroscopic, Coriolis, rotational inertia, and the centrifugal effects.

Model-based investigations of the tool holding system showed every zero-speed mode to split into two for every non-zero speed. The natural frequencies of the dominant fundamental mode of the tool holder without the absorber were observed to change by up to ~33% over the speed range of interest. And the dynamics characterized by frequency response functions (FRFs) were also observed to exhibit strong speed-dependent behavior. And due to the rotational effects coupling vibrations in orthogonal planes, the cross responses were observed to be as flexible as the direct ones. Since these responses govern the chatter-free machining stability limits, maximization of this limit was treated as the objective function to find the optimal mass, stiffness and damping of the absorber while accounting for the speed-dependent characteristics of the tool holding system.

Optimization investigations suggested that, in general, the chatter-free machining stability limits increase with an increase in the mass, stiffness, and damping of the absorber. Every combination of optimized mass, stiffness and damping of the absorber was checked to ensure that the relative forced vibration response was less than the gap between the absorber and the holder. For an optimally sized absorber, i.e., for an optimized mass, stiffness, and damping combination, peak magnitude of the most flexible mode in the direct FRF of the damped tool reduced by ~92%. For simulated cutting of Aluminium in the 50% up-milling mode and in the slot-milling mode, the optimally tuned absorber using the proposed approach was shown to result in a ~16.5 fold improvement in the chatter-free machining capability as compared to a ~11.5 fold improvement that might be possible using the classical method of tuning the absorber.

The present study ignored any potential influence of runout. Runout, if/when present, will cause centrifugal forces, and that in turn will influence the steady state response of the system and change the speed-dependent dynamic behavior of the system characterized by FRFs. That may in turn influence how the absorber might need to be tuned differently. Moreover, runout will also change the regenerative delay in the system, with one tooth potentially cutting more than others and resulting in missed cut effects. The stability model to incorporate varying multiple delays due to runout will also change. Since modeling the effects of runout will require recasting the analytical and the stability model, those investigations could be pursued in future follow-on research.

Methods herein can instruct the design and selection of elastomeric materials with higher stiffness and damping to support the absorber within the tool holder. Moreover, methods proposed are generalized enough to instruct the design and development of other chatter-resistant damped rotating slender tooling systems.

CRediT authorship contribution statement

Arjun Patel: Formal analysis, Investigation, Methodology, Software, Data curation, Validation, Visualization, Writing – review & editing. **Devang kumar Talaviya:** Formal analysis, Investigation, Methodology, Visualization, Writing – original draft. **Mohit Law:** Conceptualization, Supervision, Funding acquisition, Writing – original draft, Writing – review & editing. **Pankaj Wahi:** Conceptualization, Methodology, Supervision, Writing – review & editing.

Declaration of Competing Interest

The authors declare that they have no known competing financial interests or personal relationships that could have appeared to influence the work reported in this paper.

References

[1] W. Kim, A. Argento, R.A. Scott, Forced vibration and dynamic stability of a rotating tapered composite timoshenko shaft: bending motions in end-milling operations, J. Sound Vib. 246 (2001) 583–600, https://doi.org/10.1006/jsvi.2000.3521.
[2] J. Ma, Y. Ren, Free vibration and chatter stability of a rotating thin-walled composite bar, Adv. Mech. Eng. 10 (2018) 1–10, https://doi.org/10.1177/1687814018798265.
[3] J. Ma, J. Xu, Y. Ren, Analysis on free vibration and stability of rotating composite milling bar with large aspect ratio, Appl. Sci. (2020) 10, https://doi.org/10.3390/app10103557.
[4] Y. Liu, Z. Liu, Q. Song, B. Wang, Development of constrained layer damping toolholder to improve chatter stability in end milling, Int. J. Mech. Sci. 117 (2016) 299–308, https://doi.org/10.1016/j.ijmecsci.2016.09.003.
[5] M. Kim, J.H. Kim, M. Lee, S.K. Lee, Surface finish improvement using a damping-alloy sleeve-insert tool holder in the end milling process, Int. J. Adv. Manuf. Technol. 106 (2020) 2433–2449, https://doi.org/10.1007/s00170-019-04757-0.
[6] Y. Xia, Y. Wan, X. Luo, H. Wang, N. Gong, J. Cao, Z. Liu, Q. Song, Development of a toolholder with high dynamic stiffness for mitigating chatter and improving machining efficiency in face milling, Mech. Syst. Signal Process. 145 (2020), 106928, https://doi.org/10.1016/j.ymssp.2020.106928.
[7] Y. Xia, Y. Wan, X. Luo, H. Wang, N. Gong, J. Cao, Q. Song, Z. Liu, Chatter suppression in large overhang face milling using a toolholder with high dynamic performance, Int. J. Adv. Manuf. Technol. (2020), https://doi.org/10.1007/s00170-020-05515-3.
[8] N.H. Kim, D. Won, J.C. Ziegert, Numerical analysis and parameter study of a mechanical damper for use in long slender endmills, Int. J. Mach. Tools Manuf. 46 (2006) 500–507, https://doi.org/10.1016/j.ijmachtools.2005.07.004.
[9] R. Madoliat, S. Hayati, A.G. Ghalebahman, Sharif university of technology investigation of chatter suppression in slender endmill via a frictional damper, Sci. Iran. 18 (2011) 1069–1077, https://doi.org/10.1016/j.scient.2011.08.008.
[10] H. Moradi, F. Bakhtiari-nejad, M.R. Movahhedy, Stability improvement and regenerative chatter suppression in nonlinear milling process via tunable vibration absorber, J. Sound Vib. 331 (2012) 4668–4690, https://doi.org/10.1016/j.jsv.2012.05.032.
[11] H. Moradi, M.R. Movahhedy, G. Vossoughi, Tunable vibration absorber for improving milling stability with tool wear and process damping effects, MAMT 52 (2012) 59–77, https://doi.org/10.1016/j.mechmachtheory.2012.01.009.
[12] Y. Nakano, H. Takahara, E. Kondo, Countermeasure against chatter in end milling operations using multiple dynamic absorbers, J. Sound Vib. 332 (2013) 1626–1638, https://doi.org/10.1016/j.jsv.2012.10.035.
[13] Y. Yang, Y. Wang, Q. Liu, Design of a milling cutter with large length–diameter ratio based on embedded passive damper, JVC/Journal Vib. Control. 25 (2019) 506–516, https://doi.org/10.1177/1077546318786594.
[14] Silent Tools Damped machining tools, Sandvik Coromant. (n.d.).
[15] J.P. Den Hartog, Mechanical Vibrations, Dover Publications, New York, USA, 1985.
[16] T. Asami, O. Nishihara, A.M. Baz, Analytical solutions to h∞ and h2 optimization of dynamic vibration absorbers attached to damped linear systems, J. Vib. Acoust. Trans. ASME. 124 (2002) 284–295, https://doi.org/10.1115/1.1456458.
[17] N.D. Sims, Vibration absorbers for chatter suppression: a new analytical tuning methodology, J. Sound Vib. 301 (2007) 592–607, https://doi.org/10.1016/j.jsv.2006.10.020.
[18] E.I. Rivin, H. Kang, Enhancement of dynamic stability of cantilever tooling structures, Int. J. Mach. Tools Manuf. 32 (1992) 539–561, https://doi.org/10.1016/0890-6955(92)90044-H.
[19] Y.S. Tarng, J.Y. Kao, E.C. Lee, Chatter suppression in turning operations with a tuned vibration absorber, J. Mater. Process. Technol. 105 (2000) 55–60, https://doi.org/10.1016/S0924-0136(00)00585-9.
[20] H. Moradi, F. Bakhtiari-Nejad, M.R. Movahhedy, Tuneable vibration absorber design to suppress vibrations: an application in boring manufacturing process, J. Sound Vib. 318 (2008) 93–108, https://doi.org/10.1016/j.jsv.2008.04.001.
[21] A. Yadav, D. Talaviya, A. Bansal, M. Law, Design of chatter-resistant damped boring bars using a receptance coupling approach, J. Manuf. Mater. Process. (2020) 4, https://doi.org/10.3390/jmmp4020053.
[22] W. Ma, J. Yu, Y. Yang, Y. Wang, Optimization and tuning of passive tuned mass damper embedded in milling tool for chatter mitigation, J. Manuf. Mater. Process. 5 (2020) 2, https://doi.org/10.3390/jmmp5010002.
[23] J. Lee, C. Kim, C. Lee, C. Oh, Optimal design of multiple tuned mass dampers to reduce vibrations of a ram-type structure with varying dynamics via a control theoretic framework, ASME. J. Manuf. Sci. Eng. 142 (2020), 021009, https://doi.org/10.1115/1.4045628.
[24] M. Jorkama, R. Von Hertzen, Optimal dynamic absorber for a rotating rayleigh beam, J. Sound Vib. 217 (1998) 653–664, https://doi.org/10.1006/jsvi.1998.1763.
[25] B.O. Al-Bedoor, K.A. Moustafa, K.M. Al-Hussain, Dual dynamic absorber for the torsional vibrations of synchronous motor-driven compressors, J. Sound Vib. 220 (1999) 729–748, https://doi.org/10.1006/jsvi.1998.1975.
[26] R.O. Campos, R. Nicoletti, Vibration reduction in vertical washing machine using a rotating dynamic absorber, J. Brazilian Soc. Mech. Sci. Eng. 37 (2014) 339–348, https://doi.org/10.1007/s40430-014-0151-1.
[27] F.J. Doubrawa Filho, M.A. Luersen, C.A. Bavastri, Optimal design of viscoelastic vibration absorbers for rotating systems, JVC/Journal Vib. Control. 17 (2011) 699–710, https://doi.org/10.1177/1077546310374335.
[28] J. Tian, S.G. Hutton, Chatter instability in milling systems with flexible rotating spindles-a new theoretical approach, J. Manuf. Sci. Eng. Trans. ASME. 123 (2001) 1–9, https://doi.org/10.1115/1.1285760.
[29] M.R. Movahhedy, P. Mosaddegh, Prediction of chatter in high speed milling including gyroscopic effects, Int. J. Mach. Tools Manuf. 46 (2006) 996–1001, https://doi.org/10.1016/j.ijmachtools.2005.07.043.
[30] Y. Cao, Y. Altintas, A general method for the modeling of spindle-bearing systems, J. Mech. Des. Trans. ASME. 126 (2004) 1089–1104, https://doi.org/10.1115/1.1802311.
[31] Y. Cao, Y. Altintas, Modeling of spindle-bearing and machine tool systems for virtual simulation of milling operations, Int. J. Mach. Tools Manuf. 47 (2007) 1342–1350, https://doi.org/10.1016/j.ijmachtools.2006.08.006.

[32] A. Mokhtari, A. Mazidi, M.M. Jalili, Investigation of rotary inertial dynamic effects on chatter boundary in milling process using three-dimensional Timoshenko tool model, Proc. Inst. Mech. Eng. Part K J. Multi-Body Dyn. 233 (2019) 93–110, https://doi.org/10.1177/1464419318788504.
[33] H. Cao, B. Li, Z. He, Chatter stability of milling with speed-varying dynamics of spindles, Int. J. Mach. Tools Manuf. 52 (2012) 50–58, https://doi.org/10.1016/j.ijmachtools.2011.09.004.
[34] O. Özşahin, H.N. Özgüven, E. Budak, Analytical modeling of asymmetric multi-segment rotor – bearing systems with Timoshenko beam model including gyroscopic moments, Comput Struct 144 (2014) 119–126, https://doi.org/10.1016/j.compstruc.2014.08.001.
[35] A. Labuschagne, N.F.J. van Rensburg, A.J. van der Merwe, Comparison of linear beam theories, Math. Comput. Model. 49 (2009) 20–30, https://doi.org/10.1016/j.mcm.2008.06.006.
[36] P. Hagedorn, A. DasGupta, Vibrations and Waves in Continuous Mechanical Systems, John Wiley & Sons, Ltd, England, 2007.
[37] E. Budak, Y. Altintas, Analytical prediction of chatter stability in milling - Part I: general formulation, Am. Soc. Mech. Eng. Dyn. Syst. Control Div. DSC. (1995) 545–556, 57–1.
[38] Y. Altintas, Manufacturing automation: Metal cutting, mechanics, Machine Tool vibrations, and CNC Design, Cambridge University Press, Cambridge, UK, 2012.
[39] J.A. Nelder, R. Mead, A simplex method for function minimization, Comput. J. 7 (1965) 308–313, https://doi.org/10.1093/comjnl/7.4.308.
[40] H. Akesson, T. Smirnova, L. Hakansson, Analysis of dynamic properties of boring bars concerning different clamping conditions, Mech Syst Signal Process 23 (2009) 2629–2647, https://doi.org/10.1016/j.ymssp.2009.05.012.
[41] A.A. Thekkepat, S. Devadula, M.Law S, Identifying joint dynamics in bolted cantilevered systems under varying tightening torques and torsional excitations, J. Vib. Eng. Technol. (2021), https://doi.org/10.1007/s42417-021-00386-8.
[42] D.J. Ewins, Modal Testing - Theory, Practice and Application, Research Studies Press LTD, Baldock, Hertfordshire, England, 2000.